General Disclaimer

One or more of the Following Statements may affect this Document

- This document has been reproduced from the best copy furnished by the organizational source. It is being released in the interest of making available as much information as possible.

- This document may contain data, which exceeds the sheet parameters. It was furnished in this condition by the organizational source and is the best copy available.

- This document may contain tone-on-tone or color graphs, charts and/or pictures, which have been reproduced in black and white.

- This document is paginated as submitted by the original source.

- Portions of this document are not fully legible due to the historical nature of some of the material. However, it is the best reproduction available from the original submission.

OLD DOMINION UNIVERSITY RESEARCH FOUNDATION

DEPARTMENT OF MECHANICAL ENGINEERING AND MECHANICS
SCHOOL OF ENGINEERING
OLD DOMINION UNIVERSITY
NORFOLK, VIRGINIA

LAMINAR AND TURBULENT FLOWS OVER SPHERICALLY BLUNTED CONE AND HYPERBOLOID WITH MASSIVE SURFACE BLOWING

By

Ajay Kumar

and

S. N. Tiwari, Principal Investigator

Progress Report
For the period May 1 to October 31, 1978

Prepared for the
National Aeronautics and Space Administration
Langley Research Center
Hampton, Virginia

Under
Research Grant NSG 1464
Randolph A. Graves, Jr., Technical Monitor
Space Systems Division

January 1979

DEPARTMENT OF MECHANICAL ENGINEERING AND MECHANICS
SCHOOL OF ENGINEERING
OLD DOMINION UNIVERSITY
NORFOLK, VIRGINIA

LAMINAR AND TURBULENT FLOWS OVER SPHERICALLY BLUNTED CONE AND HYPERBOLOID WITH MASSIVE SURFACE BLOWING

By

Ajay Kumar

and

S. N. Tiwari, Principal Investigator

Progress Report
For the period May 1 to October 31, 1978

Prepared for the
National Aeronautics and Space Administration
Langley Research Center
Hampton, Virginia 23665

Under
Research Grant NSG 1464
Randolph A. Graves, Jr., Technical Monitor
Space Systems Division

Submitted by the
Old Dominion University Research Foundation
P. O. Box 6369
Norfolk, Virginia 23508

January 1979

FOREWORD

This report covers the work completed on the research project "Effects of Angle of Attack on the Coupled Radiative and Convective Heat Transfer About Blunt Planetary Entry Bodies" during the period May 1 to October 31, 1978. The work was supported by the NASA/Langley Research Center (Aerothermodynamics Branch of the Space Systems Division) through research grant NSG 1464. The grant was monitored by Dr. Randolph A. Graves, Jr. of the Space Systems Division.

TABLE OF CONTENTS

LIST OF FIGURES

LIST OF FIGURES (CONCL'D)

LAMINAR AND TURBULENT FLOWS OVER SPHERICALLY BLUNTED CONE AND HYPERBOLOID WITH MASSIVE SURFACE BLOWING

By

Ajay Kumar[1] and S. N. Tiwari[2]

SUMMARY

Numerical solutions are presented for the flow over a spherically blunted cone and hyperboloid with massive surface blowing. Time-dependent viscous shock-layer equations are used to describe the flow field. The boundary conditions on the body surface include a prescribed blowing-rate distribution. The governing equations are solved by a time-asymptotic finite-difference method. Results presented here are only for a perfect gas-type flow at zero angle of attack. Both laminar and turbulent flow solutions are obtained. It is found that the effect of the surface blowing on the laminar flow field is to smooth out the curvature discontinuity at the sphere-cone juncture point, which results in a positive pressure gradient over the body. The shock slope increases on the downstream portion of the body as the surface blowing rate is increased. The turbulent flow with surface blowing is found to redevelop a boundary-layer-like region near the surface. The effects of this boundary-layer region on the flow field and heating rates are discussed.

1. INTRODUCTION

The exploration of the outer planets requires the development of a reliable aerothermal environment to be encountered by the entry probe. The aerothermal environment is characterized by high energy flow, large heat-transfer rates to the probe's surface, and high rates of mass injection from the probe's ablative heat shield into the flow. This requires the

---

[1] Research Assistant Professor, Old Dominion University Research Foundation, P. O. Box 6369, Norfolk, Virginia 23508.

[2] Professor, Department of Mechanical Engineering and Mechanics, Old Dominion University, Norfolk, Virginia 23508.

development of computer codes which can provide coupled solutions for chemically reacting and radiating flow with massive ablating rates. Most of the coupled solutions presented so far are based on the flow over analytical bodies such as hyperboloids (ref. 1 to 3). These computer codes have difficulty in treating the realistic entry probe shape, viz, the spherically blunted cone with surface blowing. Reference 4 presents some results with surface blowing on spherically blunted cones for air, but the blowing rates considered are very low, and the blowing-rate distribution is such that it starts at the stagnation point and goes to zero at the sphere-cone juncture point. There is no blowing on the conical portion of the body. The purpose of this paper is to present the solutions for the flow over a hyperboloid and spherically blunted cone with massive surface blowing rates. Results presented here are for a perfect gas-type flow at zero angle of attack and do not include radiative heating or chemical reactions in the flow field. The same gas is injected from the surface as is in the main flow field.

The analysis of reference 5 is modified and used here. Time-dependent viscous shock-layer equations in the body-oriented coordinate system are used to describe the flow field. A time-dependent finite-difference method due to MacCormack (ref. 6) is used to solve the equations. The boundary conditions on the body surface include the surface blowing. A special central differencing of the type suggested in reference 7 is used in the tangential direction at the sphere-cone junction point to take into account the discontinuity in the surface curvature. Shock is treated as a sharp discontinuity across which shock relations are used to compute the flow quantities behind the shock. The effects of turbulence on the flow-field quantities are also studied in the presence of surface blowing. A two-layer eddy viscosity model, consisting of an inner law based upon Prandtl's mixing length concept and the Clauser-Klebanoff expression for the outer law, is used in the analysis to approximate the eddy viscosity.

It is found that the effect of the surface blowing on the laminar flow field over a sphere-cone is to smooth out the curvature discontinuity at the juncture point which results in a positive pressure gradient over the body. Shock standoff distances also exhibit similar behavior. The shock gets steeper and steeper on the downstream portion of the body as the blowing rate is increased. The laminar shock layer over the sphere-cone

in the presence of surface blowing is characterized by an inner inviscid layer, a thin shear layer, an entropy layer, and an outer inviscid layer.

The turbulent flow with surface blowing is found to redevelop a boundary-layer-like the region near the surface. The shock standoff distances are significantly reduced over the downstream part of the body, and, unlike laminar flow, the shock does not get steeper with increasing blowing. The increased gradients near the surface in the turbulent flow make the convective heating and skin friction significant even with massive blowing, whereas these quantities are negligibly small for the corresponding laminar flow. Another important effect of the formation of the boundary layer like the region near the surface is on the radiative heat flux toward the body. Reference 2 shows that the radiation blocked in the inner layer is greatly reduced for the turbulent flow, thus significantly increasing the radiative heat transfer to the body surface.

2. NOMENCLATURE

H	nondimensional total enthalpy, $H'/V_\infty'^2$
h	nondimensional specific enthalpy, $h'/V_\infty'^2$
M_∞	free-stream Mach number
$\dot{m}$	surface blowing rate, $(\rho' v')_w/(\rho_\infty' V_\infty')$
$\dot{m}_0$	surface blowing rate at the axis of symmetry
n	coordinate normal to the body, n'/R_N'
p	nondimensional pressure, $p'/\rho_\infty' V_\infty'^2$
p_∞'	free-stream pressure (N/m^2)
R	gas constant (J/k_g K)
Re	free-stream Reynolds number, $\rho_\infty' V_\infty' R_N'/\mu_\infty'$
R_N'	nose radius (m)
r	body radius normal to the body axis, r'/R_N'
s	coordinate measured along the body, s'/R_N'
T	nondimensional temperature, T'/T_∞'

T'_∞	free-stream temperature (K)
t	nondimensional time, $t'_\infty V'_\infty/R'_N$
$\bar{t}$	transformed time
u	nondimensional tangential velocity, u'/V'_∞
v	nondimensional normal velocity, v'/V'_∞
V'_∞	free-stream velocity (m/sec)
y	transformed coordinate given by equation (3)
$\bar{y}$	tranformed coordinate given by equation (6)
z	transformed coordinate given by equation (3)
$\bar{z}$	transformed coordinate given by equation (6)
β	$r + n \cos \theta$
β'	stretching factor
γ	ratio of the specific heats
δ	shock standoff distance, δ'/R'_N
θ	body angle measured from the body axis
σ	Prandtl number
σ_T	turbulent Prandtl number
λ	$1 + n\kappa$
κ	local curvature, κ'/R'_N
ρ	nondimensional density, ρ'/ρ'_∞
ρ'_∞	free-stream density (kg/m^3)
μ	nondimensional viscosity, μ'/μ'_∞
μ_T	nondimensional eddy viscosity, μ'_T/μ'_∞
μ'_∞	free-stream viscosity ($N\ sec/m^2$)
$\varepsilon+$	normalized eddy viscosity, μ_T/μ

Superscript

(')	dimensional quantities

Subscript

w	conditions at the body surface
∞	conditions in the free stream

3. ANALYSIS

The basic equations are obtained from the unsteady Navier-Stokes equations by keeping terms up to second order in the inverse square root of Reynolds number in both the viscous and inviscid regions. The body-oriented coordinate system shown in figure 1 is used. These time-dependent viscous shock-layer equations, developed in reference 5, are modified to include the turbulence and are used here to describe the flow field. The present analysis is for a perfect gas flow at zero angle of attack and does not include radiative heating or chemical reactions in the flow field.

3.1. Governing Equations

The governing equations are expressed in the nondimensional conservative form as:

$$\frac{\partial U}{\partial t} + \frac{\partial M}{\partial s} + \frac{\partial N}{\partial n} + Q = 0 \tag{1}$$

where

$$U = \lambda \begin{bmatrix} \rho \\ \rho u \\ \rho v \\ \rho H - p \end{bmatrix} \qquad M = \begin{bmatrix} \rho u \\ \rho u^2 + p \\ \rho uv \\ \rho uH \end{bmatrix}$$

$$N = \lambda \begin{bmatrix} \rho v \\ \rho uv - \frac{\mu}{Re}\left(1+\epsilon^{+}\right)\frac{\partial u}{\partial n} + \frac{\mu u \kappa}{\lambda\, Re} \\ p + \rho v^2 \\ \rho vH - \frac{\mu}{\sigma\, Re}\left(1+\epsilon^{+}\frac{\sigma}{\sigma_T}\right)\frac{\partial h}{\partial n} - \frac{\mu u}{Re}\left(1+\epsilon^{+}\right)\frac{\partial u}{\partial n} + \frac{\mu u^2 \kappa}{\lambda\, Re} \end{bmatrix}$$

$$Q = \frac{\lambda \sin\theta}{\beta} M + \frac{\cos\theta}{\beta} N$$

$$+ \frac{1}{\beta}\begin{bmatrix} 0 \\ \beta\kappa\rho uv - \frac{\mu}{Re}\left(1+\epsilon^{+}\right)\beta\kappa\frac{\partial u}{\partial n} - p\,\lambda\sin\theta + \frac{\mu u \beta \kappa^2}{\lambda\, Re} \\ -\beta\kappa\rho u^2 - p\,(\lambda\cos\theta + \beta\kappa) \\ 0 \end{bmatrix}$$

These equations are not valid at the axis of symmetry. A limiting form of the governing equations is obtained by differentiating equation (1) with respect to s and taking the limit as $s \to 0$. The following equations are obtained at the axis of symmetry:

$$\frac{\partial U_o}{\partial t} + \frac{\partial M_o}{\partial s} + \frac{\partial N_o}{\partial n} + Q_o = 0 \qquad (2)$$

where

$$U_o = \lambda \begin{bmatrix} \rho \\ \rho u \\ \rho v \\ \rho H - p \end{bmatrix} \qquad M_o = \begin{bmatrix} 2\rho u \\ p + 2\rho u^2 \\ 2\rho uv \\ 2\rho uH \end{bmatrix}$$

$$N_o = \lambda \begin{bmatrix} \rho v \\ \rho uv - \frac{\mu}{Re}\left(\frac{\partial u}{\partial n} - \frac{\mu\kappa}{\lambda}\right) - \frac{\mu\varepsilon^+}{Re}\frac{\partial u}{\partial n} \\ P + \rho v^2 \\ \rho vH - \frac{\mu}{\sigma\, Re}\frac{\partial h}{\partial n} - \frac{\mu\varepsilon^+}{\sigma_T\, Re}\frac{\partial h}{\partial n} - \frac{\mu u}{Re}\left(\frac{\partial u}{\partial n} - \frac{\mu\kappa}{\lambda}\right) - \frac{\mu\varepsilon^+}{Re}\, u\frac{\partial u}{\partial n} \end{bmatrix}$$

$$Q_o = \kappa \begin{bmatrix} \rho v \\ 2\left\{\rho uv - \frac{\mu}{Re}\left(\frac{\partial u}{\partial n} - \frac{\mu\kappa}{\lambda}\right) - \frac{\mu\varepsilon^+}{Re}\frac{\partial u}{\partial n}\right\} \\ \rho\left(v^2 - u^2\right) \\ \rho vH - \frac{\mu}{\sigma\, Re}\frac{\partial h}{\partial n} - \frac{\mu\varepsilon^+}{\sigma_T\, Re}\frac{\partial h}{\partial n} - \frac{\mu u}{Re}\left(\frac{\partial u}{\partial n} - \frac{\mu\kappa}{\lambda}\right) - \frac{\mu\varepsilon^+}{Re}\, u\frac{\partial u}{\partial n} \end{bmatrix}$$

In addition to the above equations, an equation of state and a viscosity law are used to complete the set of governing equations.

Two independent variable transformations are applied to the governing equations. The first transformation maps the computational domain into a rectangular region in which both the shock and the body are made boundary mesh lines. This transformation is given by

$$y = s,\ z = 1 - n/\delta \text{ and } t = t \tag{3}$$

where δ is the shock standoff distance. The transformed equations (1) and (2) are

$$\frac{\partial \delta U}{\partial t} + \frac{\partial \delta M}{\partial y} + \frac{\partial}{\partial z}\left[(1 - z)(\delta_t U + \delta_y M) - N\right] + \delta Q = 0 \tag{4}$$

$$\frac{\partial \delta U_o}{\partial t} + \frac{\partial \delta M_o}{\partial y} + \frac{\partial}{\partial z}\left[(1 - z)\left(\delta_t U_o + \delta_y M_o\right) - N_o\right] + \delta Q_o = 0 \qquad . \quad (5)$$

where

$$\delta y = \frac{\partial \delta}{\partial y} \quad \text{and} \quad \delta_t = \frac{\partial \delta}{\partial t}$$

The computational region is further mapped to another plane to allow higher resolution near the body surface without too much increase in the number of mesh points in the normal direction. The higher resolution near the body surface is desirable for an accurate calculation of skin-friction and heating rates. The second transformation is given by (ref. 8)

$$\bar{y} = y, \quad \bar{z} = \frac{\ell n\left(\frac{\beta' + z}{\beta' - z}\right)}{\ell n\left(\frac{\beta' + 1}{\beta' - 1}\right)} \quad \text{and} \quad \bar{t} = t \qquad (6)$$

With this transformation, the final form of equation (4) is

$$\frac{\partial U'}{\partial \bar{t}} + \frac{\partial M'}{\partial \bar{y}} + \frac{\partial N'}{\partial \bar{z}} + Q' = 0$$

where

$$U' = \delta U, \quad M' = \delta M$$

$$N' = \left(\frac{\partial \bar{z}}{\partial z}\right)\left[(1 - z)\left(\delta_{\bar{t}}\, U + \delta_{\bar{y}}\, M\right) - N\right]$$

$$Q' = \delta Q - \left(\frac{2z}{\beta'^2 - z^2}\right)\left[(1 - z)\left(\delta_{\bar{t}}\, U + \delta_{\bar{y}}\, M\right) - N\right]$$

Equation (5) can also be written in a similar form; here

$$\frac{\partial \bar{z}}{\partial z} = \frac{2\beta'}{\ell n\left(\frac{\beta' + 1}{\beta' - 1}\right)}\left(\frac{1}{\beta'^2 - z^2}\right)$$

and

$$z = \beta' \left[\left(\frac{\beta' + 1}{\beta' - 1} \right)^{\bar{z}} - 1 \right] \Big/ \left[\left(\frac{\beta' + 1}{\beta' - 1} \right)^{\bar{z}} + 1 \right]$$

The partial derivative with respect to n in the expressions for N and Q are to be replaced by

$$\frac{\partial}{\partial n} = -\frac{1}{\delta} \frac{\partial}{\partial z} = -\frac{1}{\delta} \left(\frac{\partial \bar{z}}{\partial z} \right) \frac{\partial}{\partial \bar{z}}$$

3.2. Boundary Conditions

The boundary conditions at the shock are calculated by using the shock relations. At the wall, no slip conditions are used. The wall temperature is taken as a specified value, and a prescribed blowing rate distribution is used on the surface.

3.3. Eddy Viscosity Approximation

A two-layer eddy viscosity model consisting of an inner law and an outer law is used in the present analysis. This model, introduced by Cebeci (ref. 9), assumes that the inner law is applicable for the flow from the wall out to the location where the eddy viscosity given by the inner law is equal to that of the outer law. The outer law is then assumed to be applicable for the rest of the shock layer. The expressions for the inner and outer laws are given below.

3.3.1. Inner Eddy Viscosity Approximation. - Prandtl's mixing-length concept is stated in nondimensional variables as

$$\varepsilon_i^+ = \frac{\rho \ell^2 Re}{\mu} \left| \frac{\partial u}{\partial n} \right| \tag{7}$$

The mixing length ℓ is evaluated from the expression

$$\ell = k_1 n [1 - \exp(-n^+/A^+)]$$

where

$$n^+ = \frac{n\rho}{\mu}\left[\frac{\mu_w \, Re}{\rho}\left(\frac{\partial u}{\partial n}\right)_w\right]^{1/2}$$

Here, k_1 is the Von Kármán constant, which is assumed to have a value of 0.4, and A^+ is a damping factor which is expressed as

$$A^+ = 26 \exp(-5.9\, v^+)$$

where

$$v^+ = v_w/u_\tau$$

and

$$u_\tau = \left[\frac{\mu_w}{\rho Re}\left(\frac{\partial u}{\partial n}\right)_w\right]^{1/2}$$

2.3.2. Outer Eddy Viscosity Approximation. - For the outer region of the viscous layer, the eddy viscosity is approximated by the Clauser-Klebanoff expression (based on refs. 10 and 11):

$$\varepsilon_o{}^+ = \frac{k_2 \, \rho \, u_e \, Re \, \delta_k \, \gamma_{i,n}}{\mu} \tag{8}$$

where

$$\delta_k = \int_0^{\delta_b}\left(1 - \frac{u}{u_e}\right)dn$$

$$k_2 = 0.0168$$

and

$$\gamma_{i,\eta} = [1 + 5.5\ (n/\delta_b)^6]^{-1}$$

Here, δ_b is the boundary-layer thickness and u_e is the local value at the edge of the boundary layer. The expression for $\gamma_{i,\eta}$ is Cebeci's approximation of the error-function definition presented by Klebanoff (ref. 11). The boundary-layer thickness δ_b is assumed to be the value of n at the point where

$$\frac{H}{H_\infty} = 0.995$$

In the present analysis, the turbulent Prandtl number is assumed to be 0.9.

4. METHOD OF SOLUTION

MacCormack's two-step finite-difference method (ref. 6) is used to solve the governing equations. This explicit method has second-order accuracy in both space and time and is highly efficient on the CDC-STAR-100 computer. Since only the steady-state solution is of interest in the present investigation, the solution is marched in time on each mesh point according to its largest possible Courant-Friedrich-Lewy (CFL) time-step size. It is shown in reference 12 that the use of local time-step results in a speedup of two or or more over the regular MacCormack scheme in which the solution is marched with global minimum CFL time-step on all the mesh points. Due to these reasons, the present analysis still uses the original MacCormack scheme although several more recent versions are available.

In addition to the instability which will occur if the maximum allowable time-step is exceeded, it is found that the present solutions exhibited large oscillations across the shock layer. A fourth-order damping technique is used to damp these oscillations. The details of the method are given in reference 5.

A special central differencing of the type suggested in reference 7 is used in the tangential direction at the sphere-cone juncture point to take into account the discontinuity in the surface curvature.

5. DISCUSSION OF RESULTS

Flow-field results are presented for the forebody of hyperboloids and spherically blunted cones with massive surface blowing. Results are presented for both laminar and turbulent flow. Two different sets of conditions are used. These conditions are given below.

I. Gas : Air

$M_\infty = 10.33$ $\qquad$ $T'_w = 330.6$ K

$T'_\infty = 46.26$ K $\qquad$ $\gamma = 1.4$

$p'_\infty = 100.77$ N/m^2 $\qquad$ $\sigma = 0.7$

$R'_N = 0.03175$ m $\qquad$ Re = 115800

$\mu' = 1.458 \times 10^{-6} \left\{(T')^{1.5}/(110 + T')\right\}$ N·sec/m^2

$R = 287$ J/k$_g$ K

The surface blowing rate distribution used with these conditions is given by

$$\dot{m}/\dot{m}_0 = (\rho v)_w/(\rho v)_{w,\ s=0} = \left[2 - 0.3\ s + \left(\cos \frac{\pi s}{4}\right)^6\right] \Big/ 3$$

These conditions and surface blowing rates are identical to those used in reference 3 and are used to obtain the laminar flow-field results over a 45-degree half-angle hyperboloid only.

II. Gas : Hydrogen-Helium Mixture (under perfect gas assumption)

$M_\infty = 43.84$ $\qquad$ $T'_w = 4000$ K

$T'_\infty = 145$ K $\qquad$ $\gamma = 1.224$

$\rho'_\infty = 1.27E - 4$ kg/m^3 $\qquad$ $\sigma = 0.72$

$R'_N = 0.222$ m $\qquad$ Re = 156700

$$\mu' = 2.48 \times 10^{-7}(T')^{0.65} \ N \cdot sec/m^2$$

$$R = 3593.6 \ J/k_g \ K$$

These conditions correspond to typical Jovian entry conditions. The surface blowing rate distribution used with these conditions is shown in figure 2. This set of conditions is used with both the spherically blunted cone and hyperboloid to obtain the laminar and turbulent flow-field results.

Results of the first set of conditions are discussed first. Figure 3 shows the effect of surface blowing on the shock standoff distance. It is seen from this figure that the shock standoff distance increases with increasing blowing rates and the shock becomes progressively steeper for the downstream points. Figure 4 shows the corresponding surface pressures which also increase with increasing blowing rates for the downstream points. Thus, the net effect of the mass injection is to produce effectively a blunter body.

The results of the present analysis are compared with those of reference 3. It is seen from figures 3 and 4 that the results of the two analyses agree very well for zero blowing but the difference increases with increasing blowing rates. For $\dot{m}_0 = 0.8$, the difference is the order of 30 percent in both the shock standoff distances and surface pressures. No reason could be attributed to these large differences. Both the analyses use the same governing equations and input conditions. The only difference is in the method of solution.

It is mentioned in reference 3 that the viscous shock-layer equations are not extendable to massive blowing rates and that it is necessary to use full Navier-Stokes equations with massive blowing. It is found in the present analysis that the viscous shock-layer equations can very well handle the massive surface blowing rates. In fact, the results obtained in the present analysis with viscous shock-layer equations and full Navier-Stokes equations are almost identical for the entire range of $\dot{m}_0$ from 0 to 0.8.

Figures 5 to 7 show the profiles for tangential velocity, enthalpy, and normal velocity at s = 0.9. Figures 5 and 6 show the typical behavior of the shock layer in the presence of surface blowing. It is characterized by an inner inviscid layer, a thin shear layer in which most of the changes

occur, and an outer inviscid layer. The extent of the inner inviscid layer increases with the increasing blowing rates. In the case of an ablating surface, this inner inviscid layer will mainly be containing the ablation gas.

The normal velocity profiles in figure 7 show that the normal velocity decreases slightly in the inner inviscid layer, increases in the shear layer, and then decreases monotonically to the shock value in the outer inviscid layer. This behavior of the normal velocity has been reported in reference 3. The increase in the normal velocity in the shear layer would enhance the mixing of the inner and outer layer gases, thus increasing the thickness of the ablation gas layer. This increase in the ablation-layer thickness is particularly important since most of the attenuation of the radiation takes place in this region.

Part of this section will now discuss the results from the second set of conditions. Results of the laminar flow are discussed first. Figure 8 shows the surface pressure distribution over a 45-degree half-angle sphere-cone with increasing surface blowing. It is seen from this figure that for zero blowing there is a negative pressure gradient on the conical portion of the body due to the discontinuity in the curvature at the juncture point. As the blowing rate is increased to $\dot{m}_0 = 0.2$, the negative pressure gradient is reduced to a very small value. For $\dot{m}_0 = 0.4$ and higher, the pressure gradient becomes positive. Thus, the effect of the surface blowing on a sphere-cone is to smooth out the curvature discontinuity at the juncture point which results in a positive pressure gradient over the body.

Shock standoff distances are shown in figure 9. This figure also shows the smoothing out of the curvature discontinuity with increasing blowing. It is also seen that the shock gets steeper and steeper as the blowing rate is increased. It did not create any problem for the present conditions and body shape, but the flow can become subsonic behind the shock for large angle bodies at downstream points.

Figures 10 through 12 show the profiles of tangential velocity enthalpy and normal velocity at s = 0.19635 for the 45-degree half-angle sphere-cone with $\dot{m}_0$ increasing from 0 to 0.6. Profiles at s = 0.19635 are also plotted in figures 13 through 15 for a 45-degree half-angle hyperboloid using the second set of conditions with $\dot{m}_0 = 0$ and 0.4. It is seen that, in the nose

region, the profiles for the sphere-cone are very similar to that for the hyperboloid. The normal velocity profile for the sphere-cone also shows the same behavior as was seen for the hyperboloid, i.e., it decreases slightly in the inner inviscid layer, increases in the thin shear layer, and then decreases monotonically to the shock value in the outer inviscid layer.

Tangential velocity, enthalpy and normal velocity profiles are plotted at s = 1.76715 in figures 16 through 21 for both the sphere-cone and hyperboloids with increasing $\dot{m}_0$. It is seen from figure 17 that, for the sphere-cone, the enthalpy changes rapidly in the inner portion of the outer inviscid layer forming an entropy layer. For the hyperboloid, the flow quantities change gradually to the shock value in the outer inviscid layer. This difference in the profiles for the two bodies will have an effect on the radiative heating.

The effect of turbulence on the flow field over the sphere-cone is discussed in the presence of surface injection. For the turbulent solutions, the flow is assumed to undergo instantaneous transition at s = 0.19635. Figure 22 shows the surface pressure distribution for the laminar and turbulent flows. For zero blowing, the surface pressures are almost identical in the laminar and turbulent flows. For $\dot{m}_0 = 0.4$, the laminar flow shows a positive pressure gradient, whereas the turbulent flow develops again a negative pressure gradient similar to that for zero blowing.

Figure 23 shows the shock standoff distances for laminar and turbulent flows. Here again, the shock standoff distances for laminar and turbulent flows are almost identical for zero blowing. For nonzero blowing, there is a significant decrease in the shock standoff distances for the turbulent flow at downstream points. Moreover, the shock slope for the turbulent flow is not seen to increase with increasing blowing rates. The figure shows that, for the turbulent flow, the shock is just pushed away from the body in the presence of blowing but the shock shape remains similar to that for zero blowing. The reduction in the shock standoff distance can be explained from figure 16 in which the turbulent tangential velocity profile for $\dot{m}_0 = 0.4$ is plotted along with the laminar profiles. The magnitude of the tangential velocity is higher all across the shock layer for the turbulent flow, which results in the reduction of the shock standoff distances. The turbulent tangential velocity profile also shows the formation of a boundary-

layer-like region near the surface. Corresponding changes in the turbulent enthalpy profile are seen in figure 17 where the enthalpy near the surface goes up for the turbulent flow. The turbulent enthalpy profile also shows a reduction in the gradients in the entropy layer due to the fact that the shock is relatively less strong for the turbulent flow than for the laminar flow. The increased gradients near the surface in the turbulent flow make the convective heating and skin friction significant even with massive blowing whereas these are negligibly small for the corresponding laminar flow.

Another very important effect of the formation of the boundary-layer-like region is on the radiative heat flux toward the body. It is discussed in reference 2 for the coupled flow-field solutions over a hyperboloid for Jovian entry. Due to the formation of a high-temperature ablation layer near the surface, the radiation blocked in the ablation layer is greatly reduced for the turbulent flow, which significantly increases the radiative heat transfer to the body surface.

Figure 24 shows the eddy viscosity distribution across the shock layer at s = 1.76715 for the 45-degree half-angle sphere-cone with $\dot{m}_0$ = 0, 0.2, and 0.4. It is seen from this figure that the eddy viscosity increases sharply with the increasing surface blowing. The two-layer model provides good approximation of the eddy viscosity for zero or small blowing rates, but the validity of this model with massive surface blowing is not known. However, it is shown in reference 2 that even if the two-layer model is assumed to be in error by a factor of 10, the radiation heat flux to the Jovian entry probe is substantially increased.

6. CONCLUSIONS

Numerical solutions for the laminar and turbulent flow over a spherically blunted cone and hyperboloid are presented with massive surface blowing. It is found that the effect of the surface blowing on the laminar flow field over a sphere-cone is to smooth out the curvature discontinuity at the juncture point, which results in a positive pressure gradient over the body. The shock slope increases at the downstream points with increasing surface blowing. The turbulent flow with surface blowing is found to redevelop a boundary-

layer-like region near the surface. The increased gradients near the surface in this boundary-layer-like region make the convective heating and skin friction significant even with massive blowing. The shock standoff distances are significantly reduced over the downstream part of the body which make the shock relatively less strong for the turbulent flow than for the laminar flow.

Results presented here are for the perfect gas-type flow and do not include radiative heating or chemical reactions in the flow field. The main purpose of this report is to demonstrate the capability of the present computer code in providing the solutions for the flow over a realistic probe shape with massive surface blowing. The code will be modified to provide the coupled solutions for the chemically reacting and radiating flow with surface ablation.

REFERENCES

1. Moss, J.N.: Radiative Viscous-Shock-Layer Solutions with Coupled Ablation Injection. AIAA, Vol. 14, No. 9, Sept. 1976, pp. 1311-1317.

2. Moss, J.N.; Anderson, E.C.; and Simmonds, A.L.: The Impact of Turbulence on a Radiating Shock Layer with Coupled Ablation Injection. AIAA Paper No. 78-1186, July 1978.

3. Graves, R.A., Jr.: Solutions to the Navier-Stokes Equations for Supersonic Flow over Blunt Bodies with Massive Blowing. Ph.D. Dissertation, George Washington University, (Washington, D.C.), Nov. 1977.

4. Gogineni, P.R.; Murray, A.L.; and Lewis, C.L.: Viscous Flows over Slender Spherically Blunted Cones at Large Angle of Attack Including Mass-Transfer and Low Reynolds Number Effects. AIAA Paper No. 78-1188, July 1978.

5. Kumar, Ajay; and Graves, R.A., Jr.: Numerical Solution of the Viscous Hypersonic Flow Past Blunted Cones at Angle of Attack. AIAA Paper No. 77-172, Jan. 1977; also AIAA, Vol. 15, No. 8, Aug. 1977, pp. 1061-1062.

6. MacCormack, R.W.: The Effect of Viscosity in Hypervelocity Impact Cratering. AIAA Paper No. 69-354, Apr. 1969.

7. Srivastava, B.N.; Werle, M.J.; and Davis, R.T.: Viscous Shock-Layer Solutions for Hypersonic Sphere-Cones. AIAA, Vol. 16, No. 2, Feb. 1978, pp. 137-144.

8. Roberts, G.O.: Computational Meshes for Boundary Layer Problems. Lecture Notes in Physics, Springer-Verlag, (NY), 1971, pp. 171-177.

9. Cebeci, T.: Behavior of Turbulent Flow near a Porous Wall with Pressure Gradient. AIAA, Vol. 8, No. 12, Dec. 1970, pp. 2152-2156.

10. Clauser, F.H.: The Turbulent Boundary Layer. Vol. IV of Advances in Applied Mathematics, H.L. Dryden and Th. Von Kármán (eds.). Academic Press, Inc., 1956, pp. 1-51.

11. Klebanoff, P.S.: Characteristics of Turbulence in a Boundary Layer with Zero Pressure Gradient. NACA Report No. 1247, 1955.

12. Kumar, Ajay; and Graves, R.A., Jr.: Comparative Study of the Convergence Rates of Two Numerical Techniques. AIAA, Vol. 16, No. 11, Nov. 1978, pp. 1214-1216.

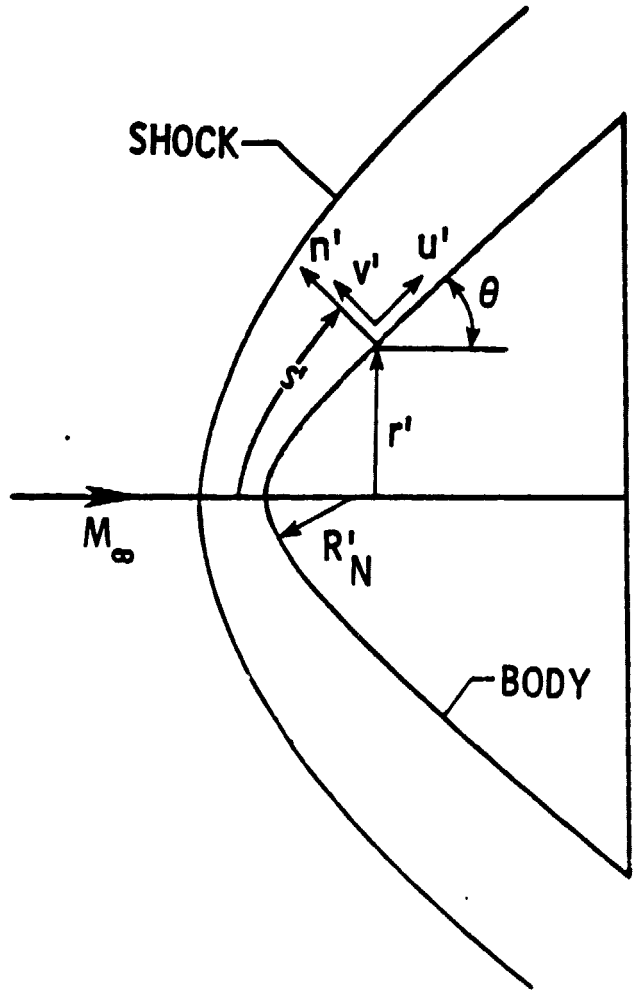

Figure 1. Coordinate system.

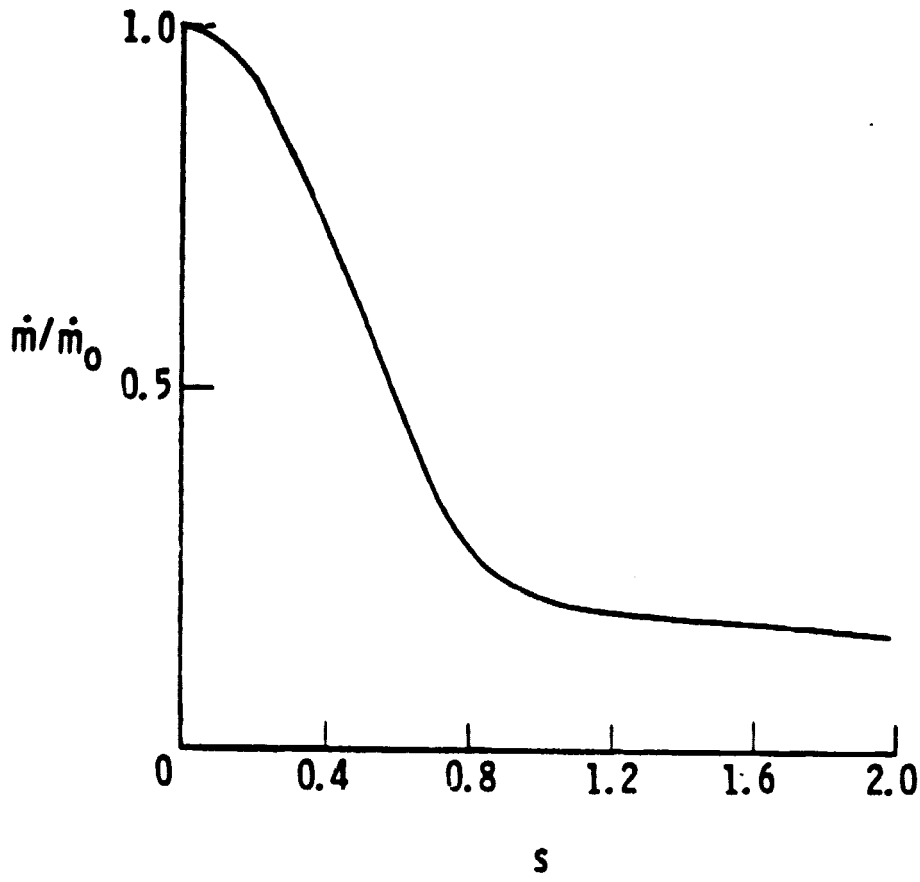

Figure 2. Surface blowing rate distribution.

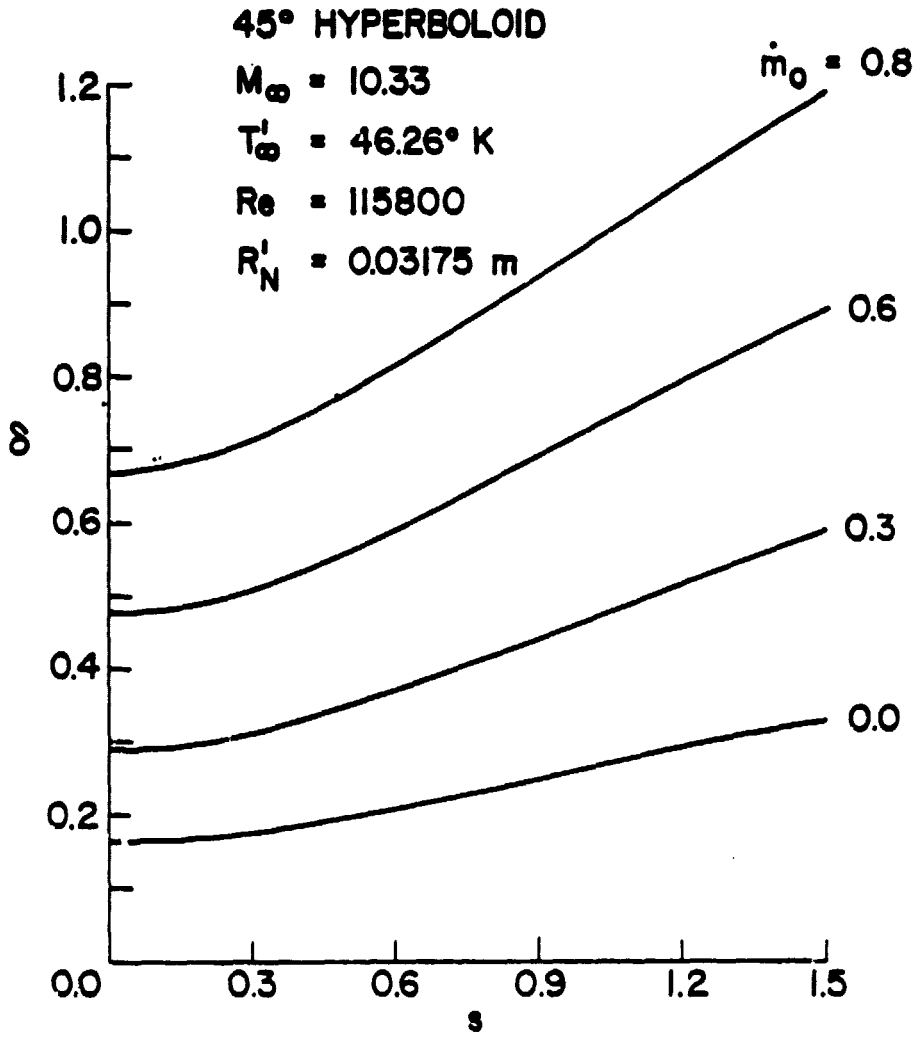

Figure 3. Shock standoff distances with surface blowing.

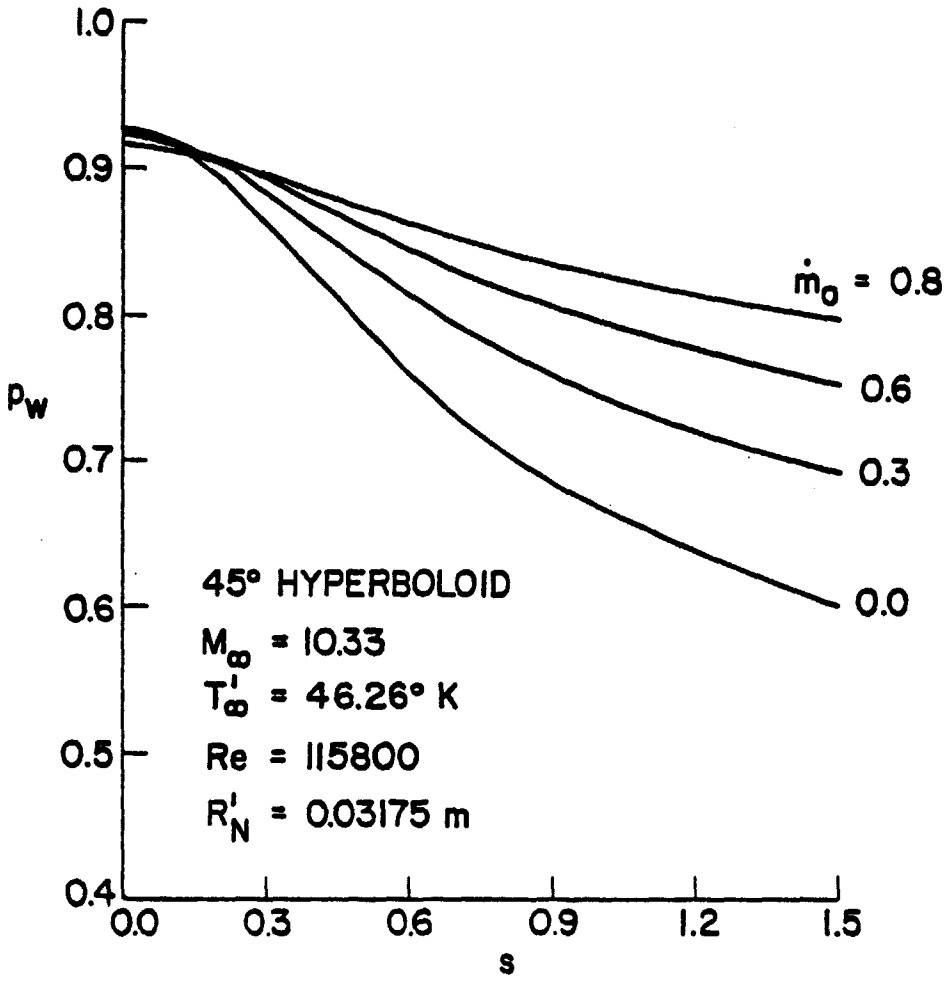

Figure 4. Surface pressure distribution with surface blowing.

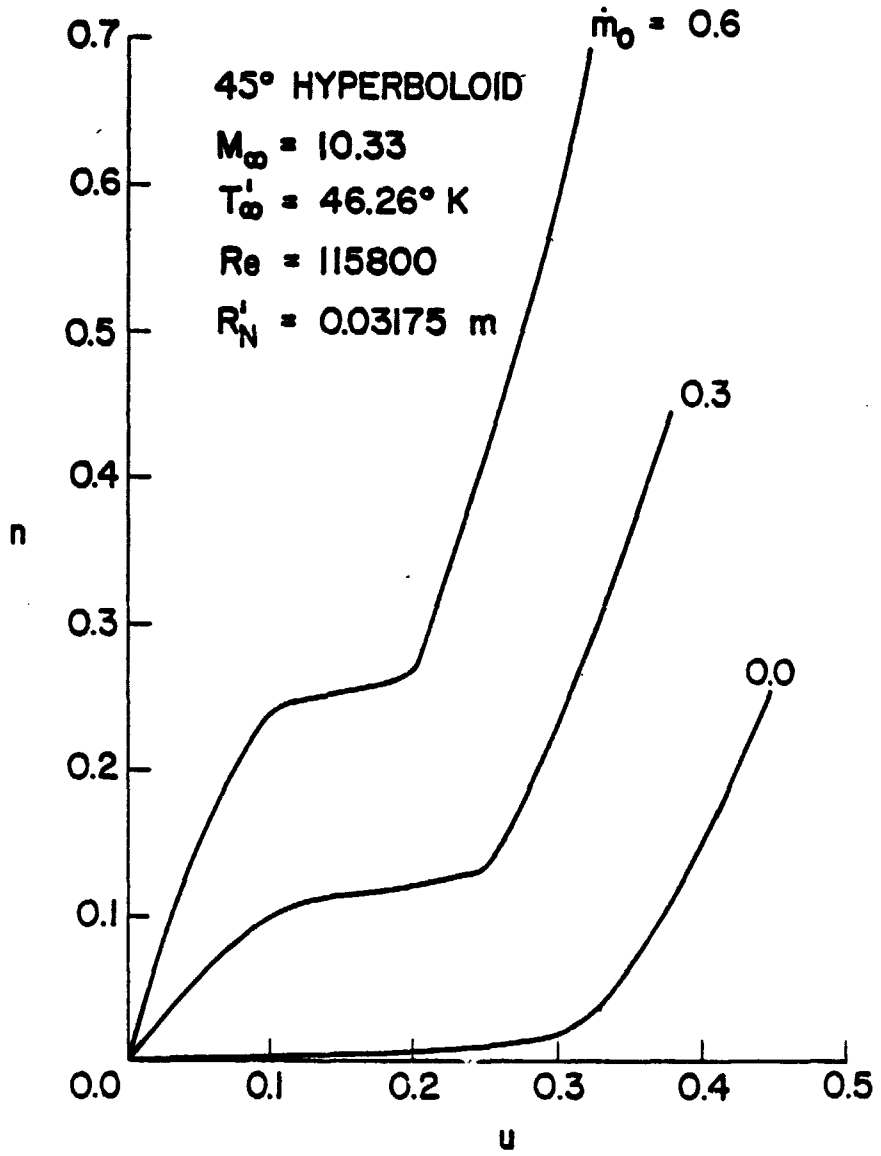

Figure 5. Tangential velocity profile variation with surface blowing at s = 0.9.

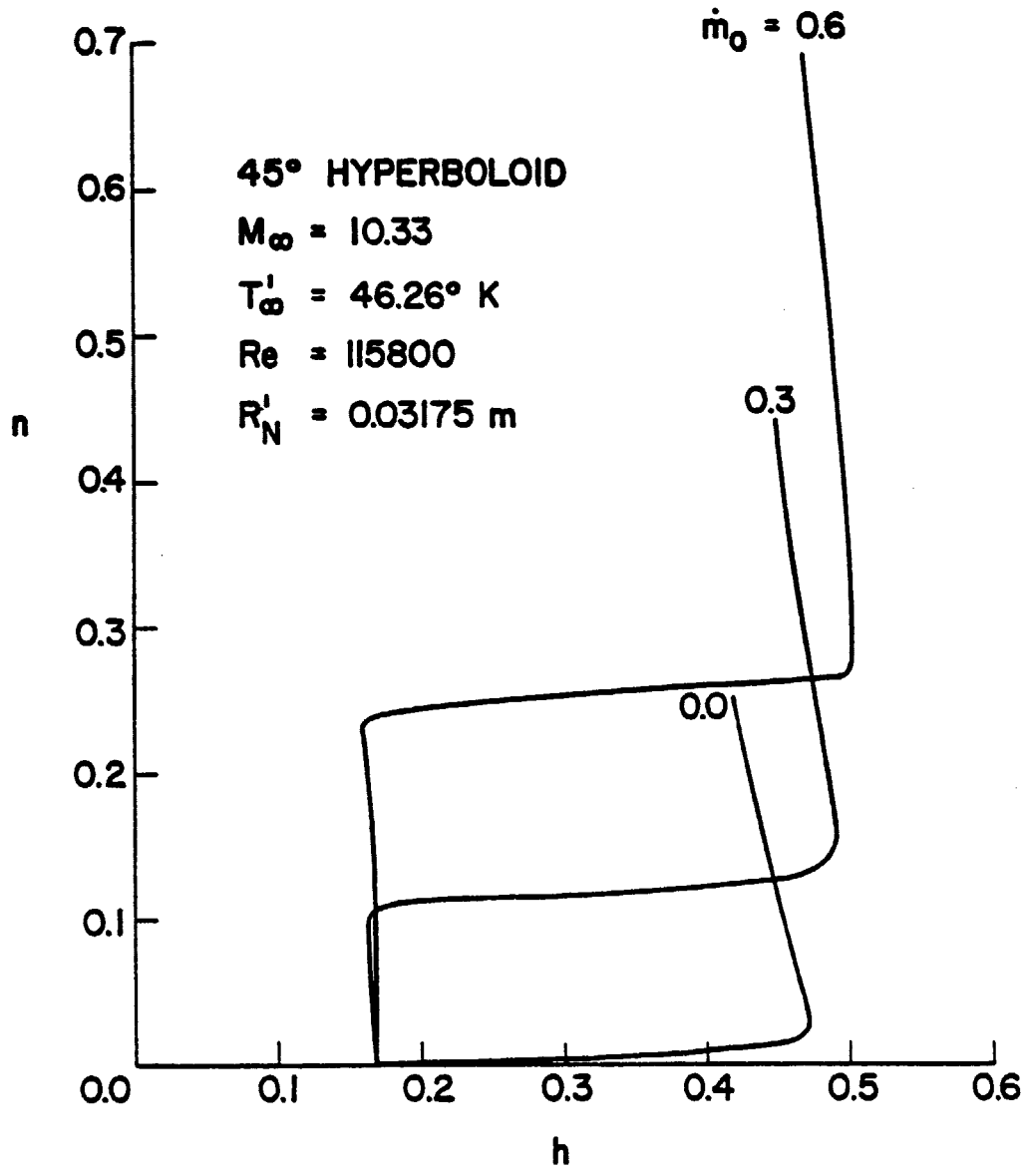

Figure 6. Enthalpy profile variation with surface blowing at s = 0.9.

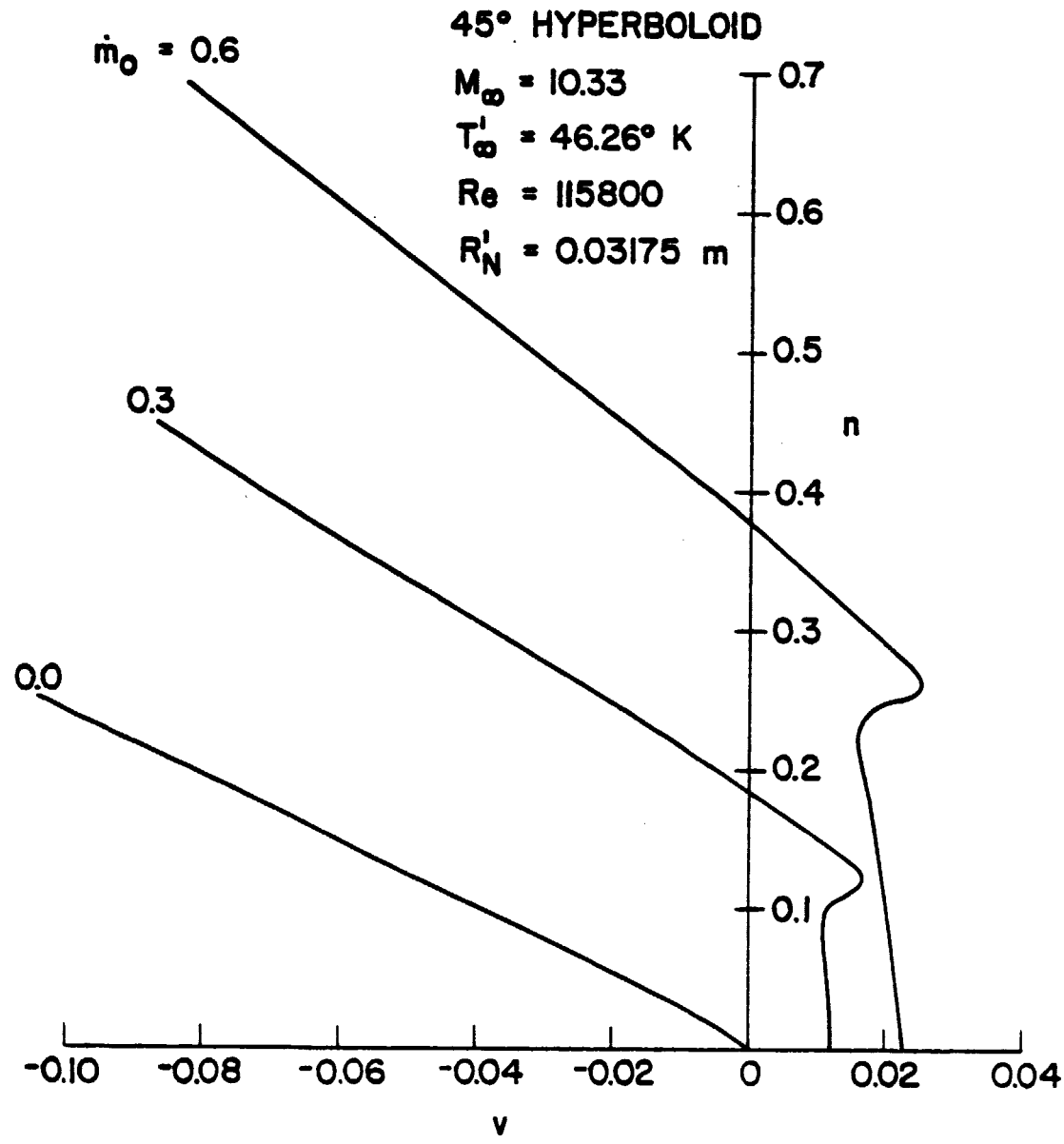

Figure 7. Normal velocity profile variation with surface blowing at s = 0.9.

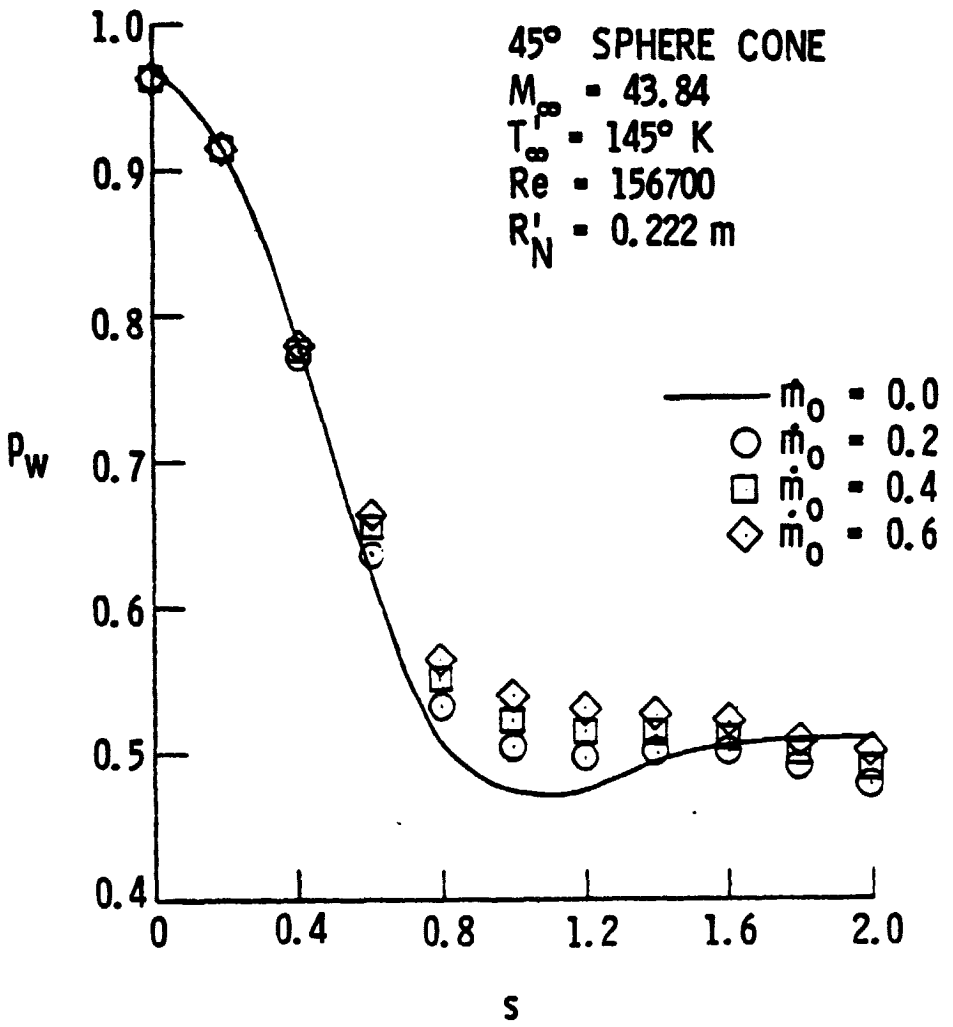

Figure 8. Surface pressure distribution with surface blowing.

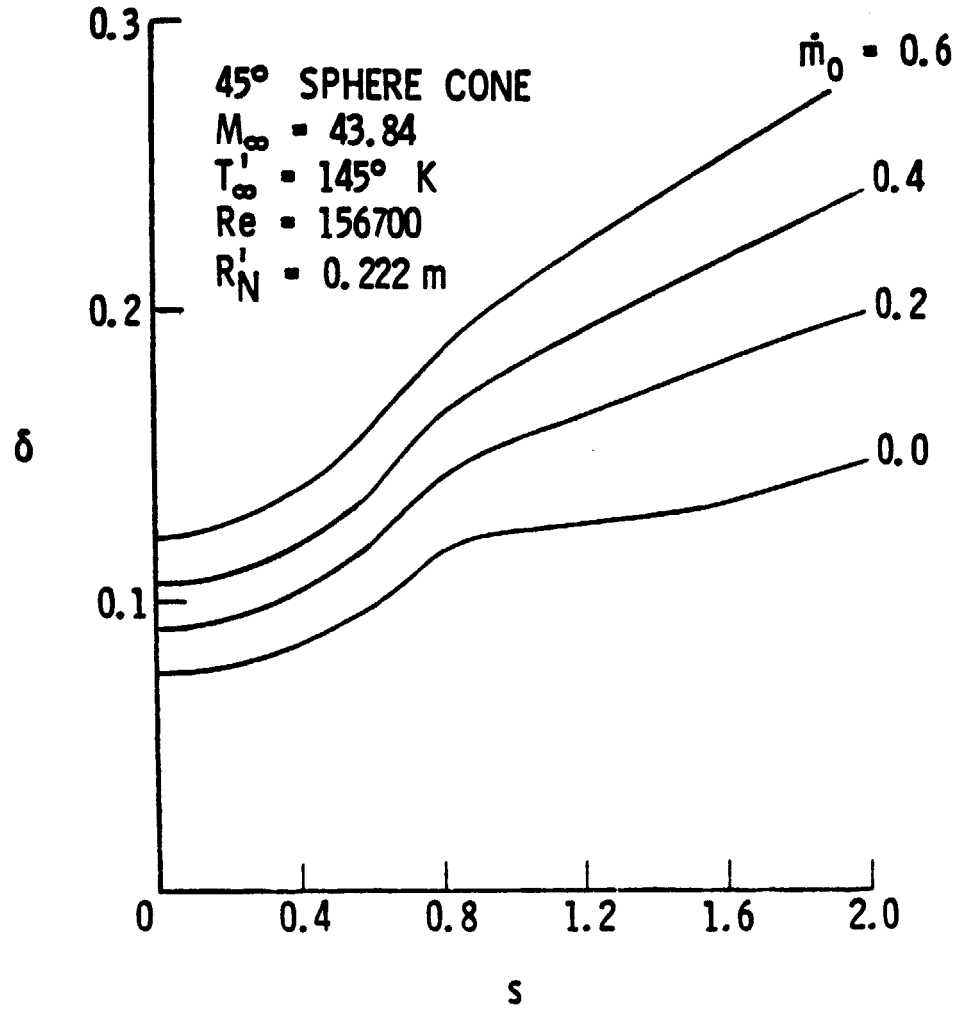

Figure 9. Shock standoff distances with surface blowing.

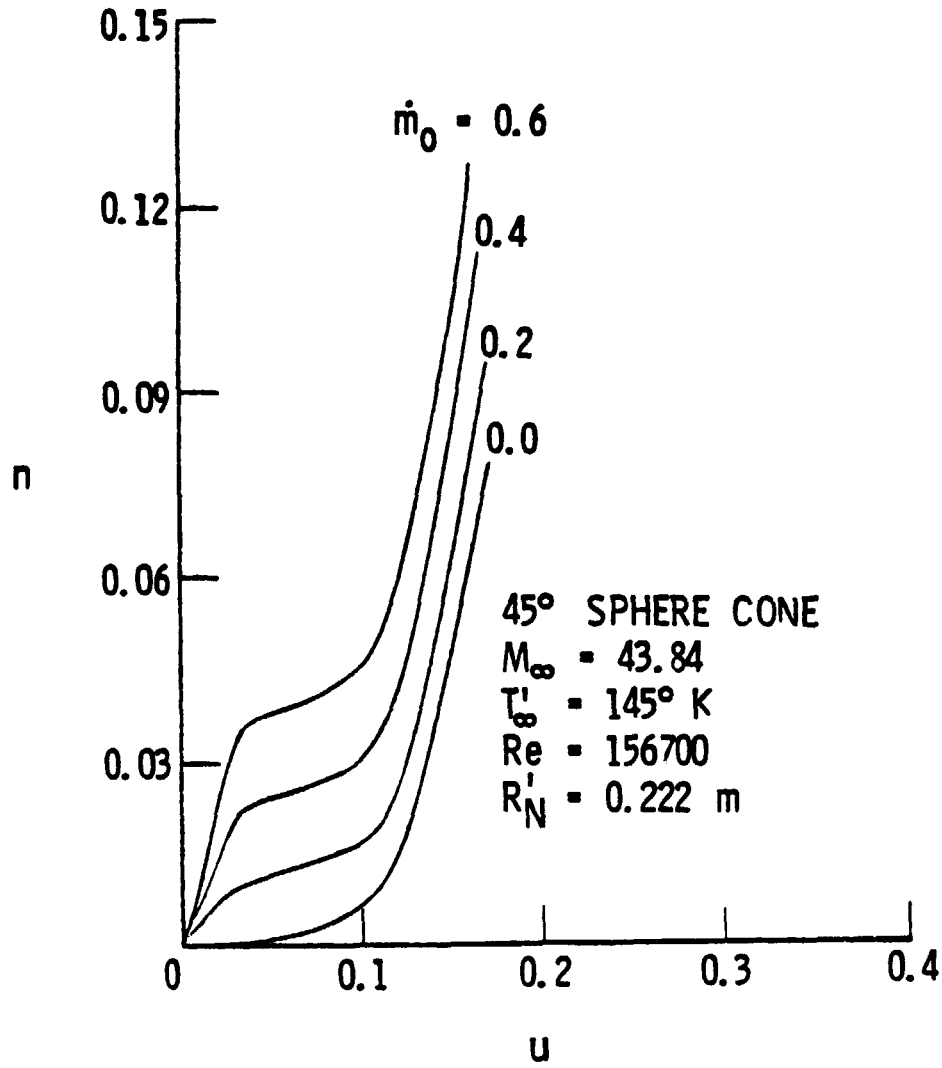

Figure 10. Tangential velocity profile variation with surface blowing at s = 0.19635.

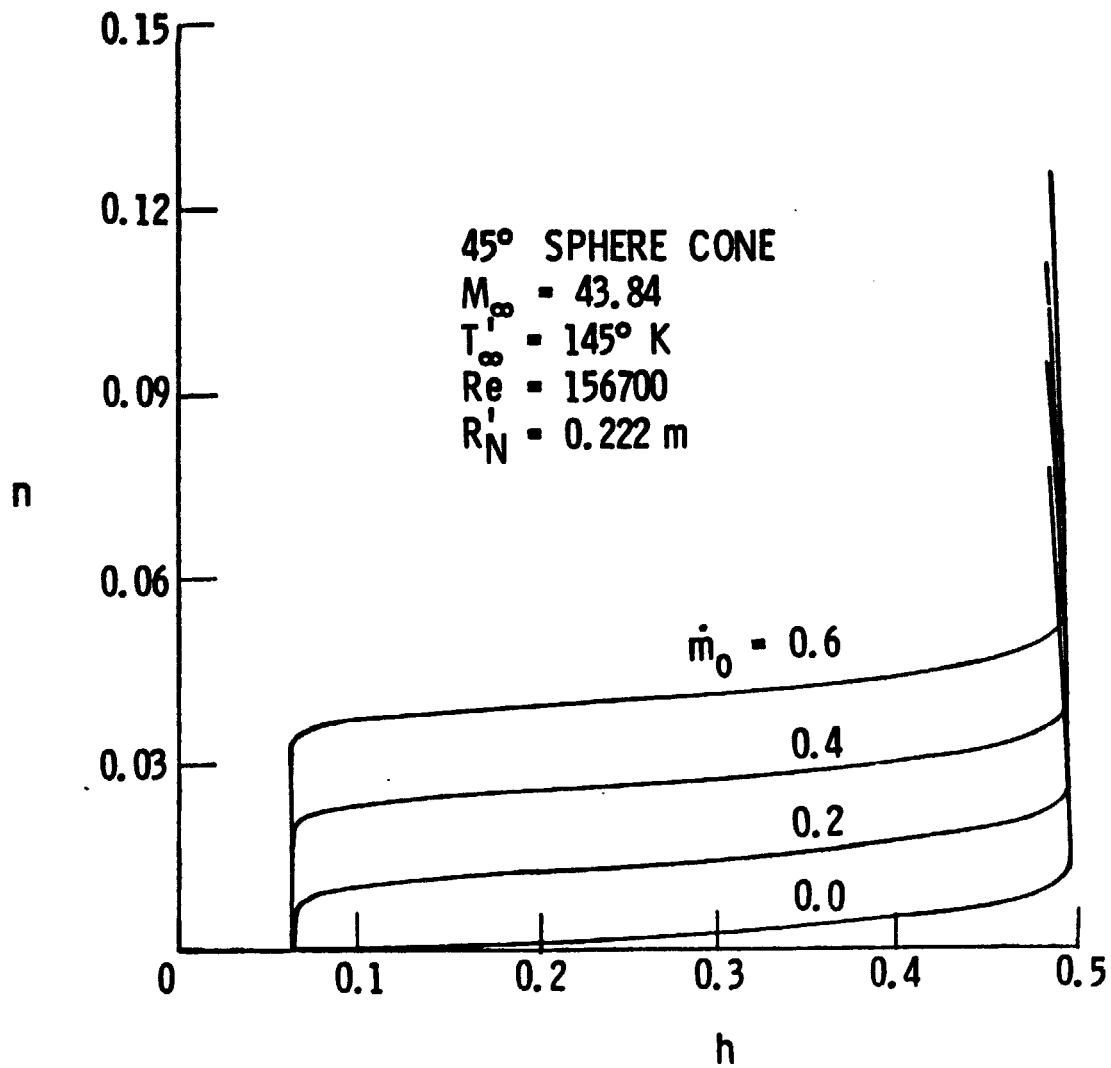

Figure 11. Enthalpy profile variation with surface blowing at s = 0.19635.

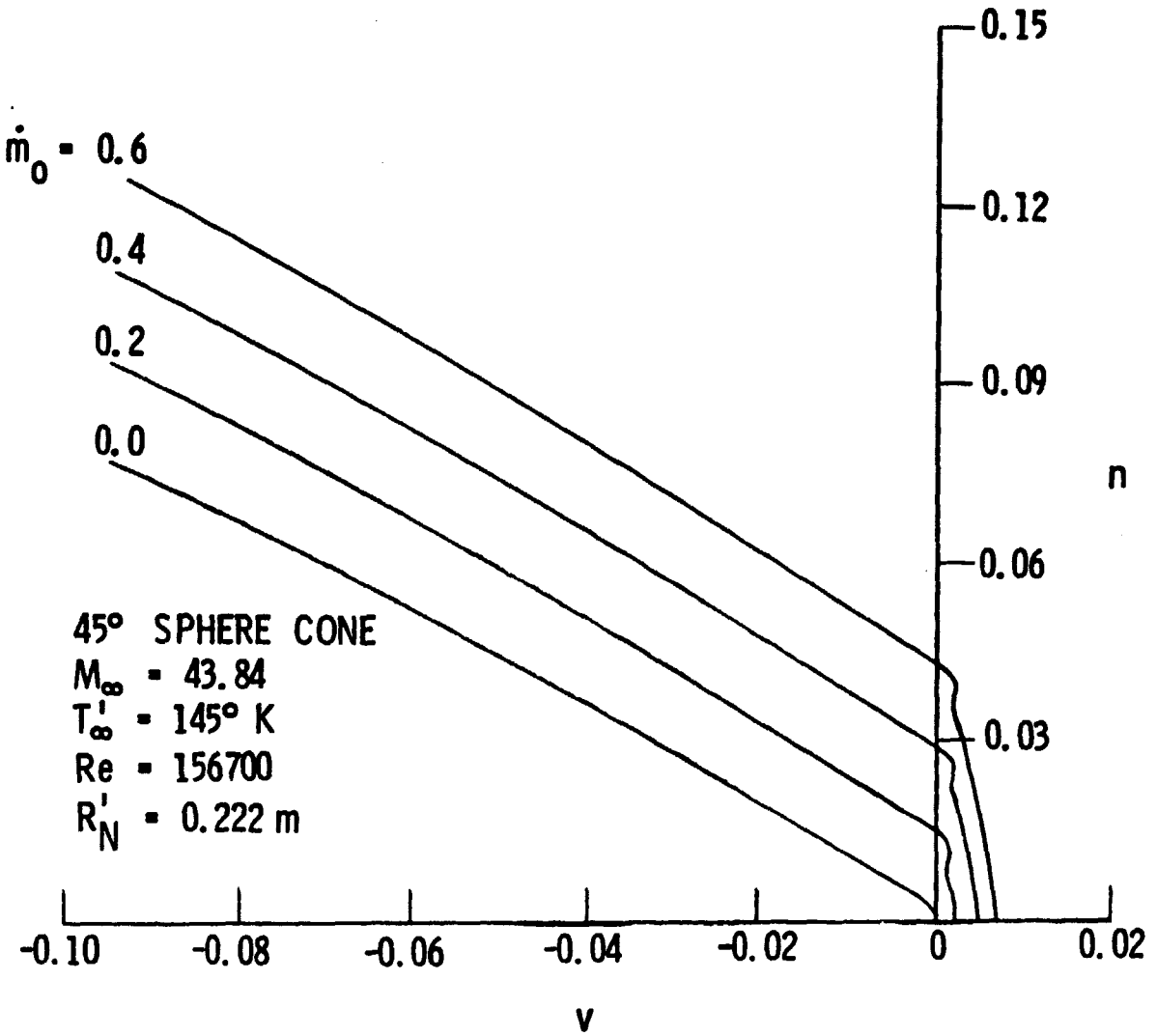

Figure 12. Normal velocity profile variation with surface blowing at s = 0.19635.

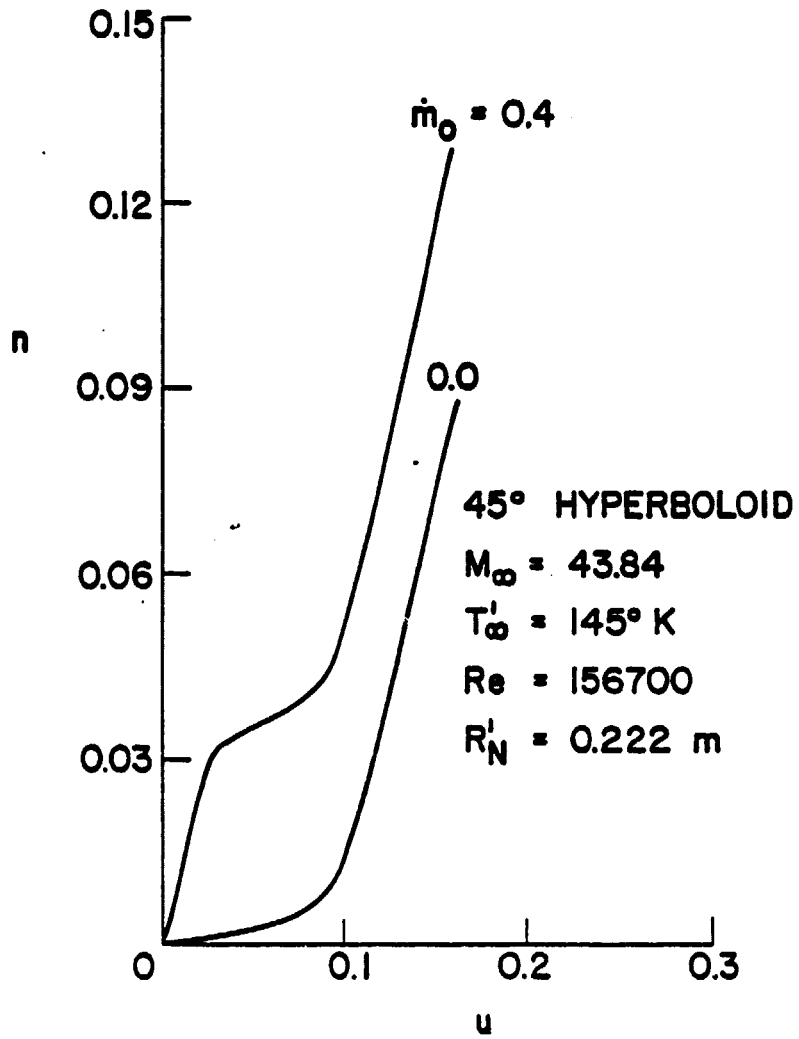

Figure 13. Tangential velocity profile variation with surface blowing at s = 0.19635.

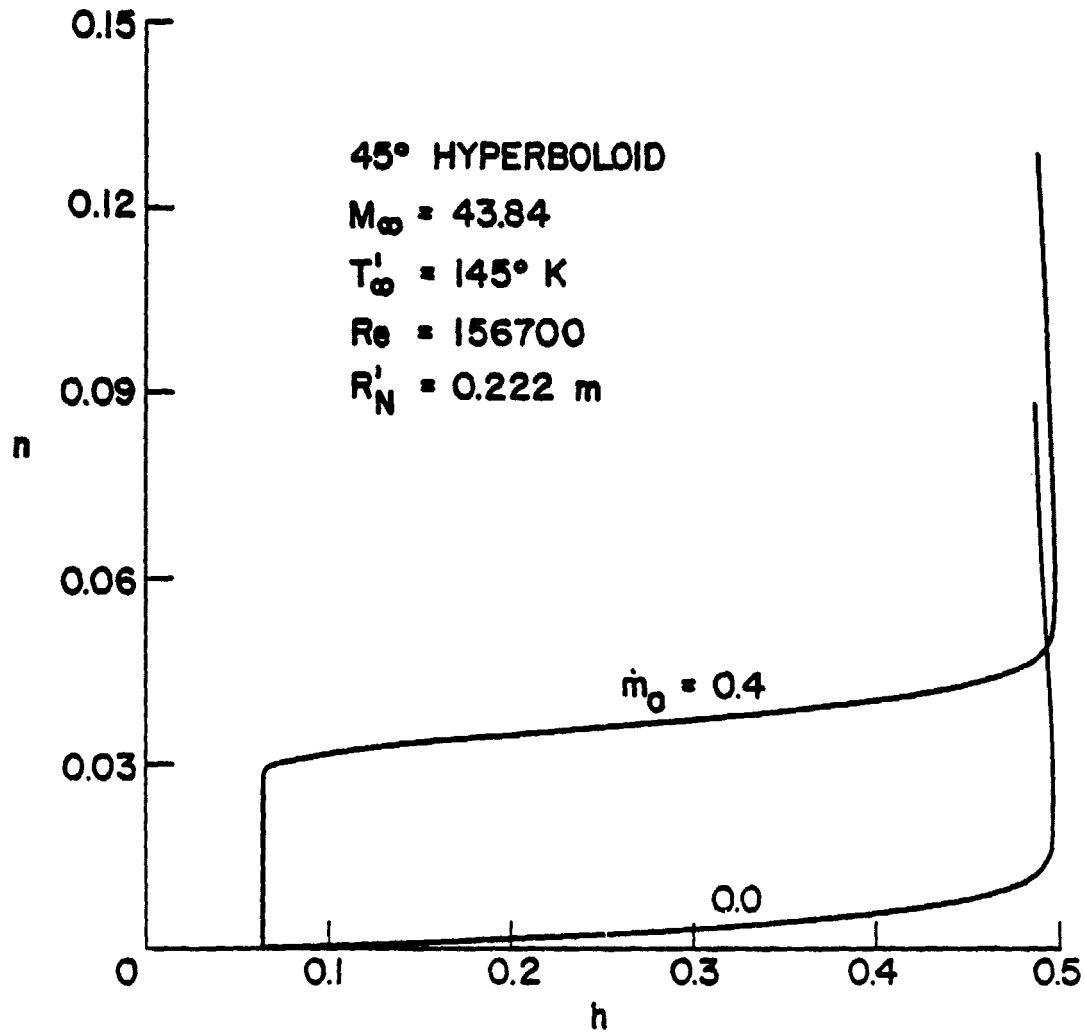

Figure 14. Enthalpy profile variation with surface blowing at s = 0.19635.

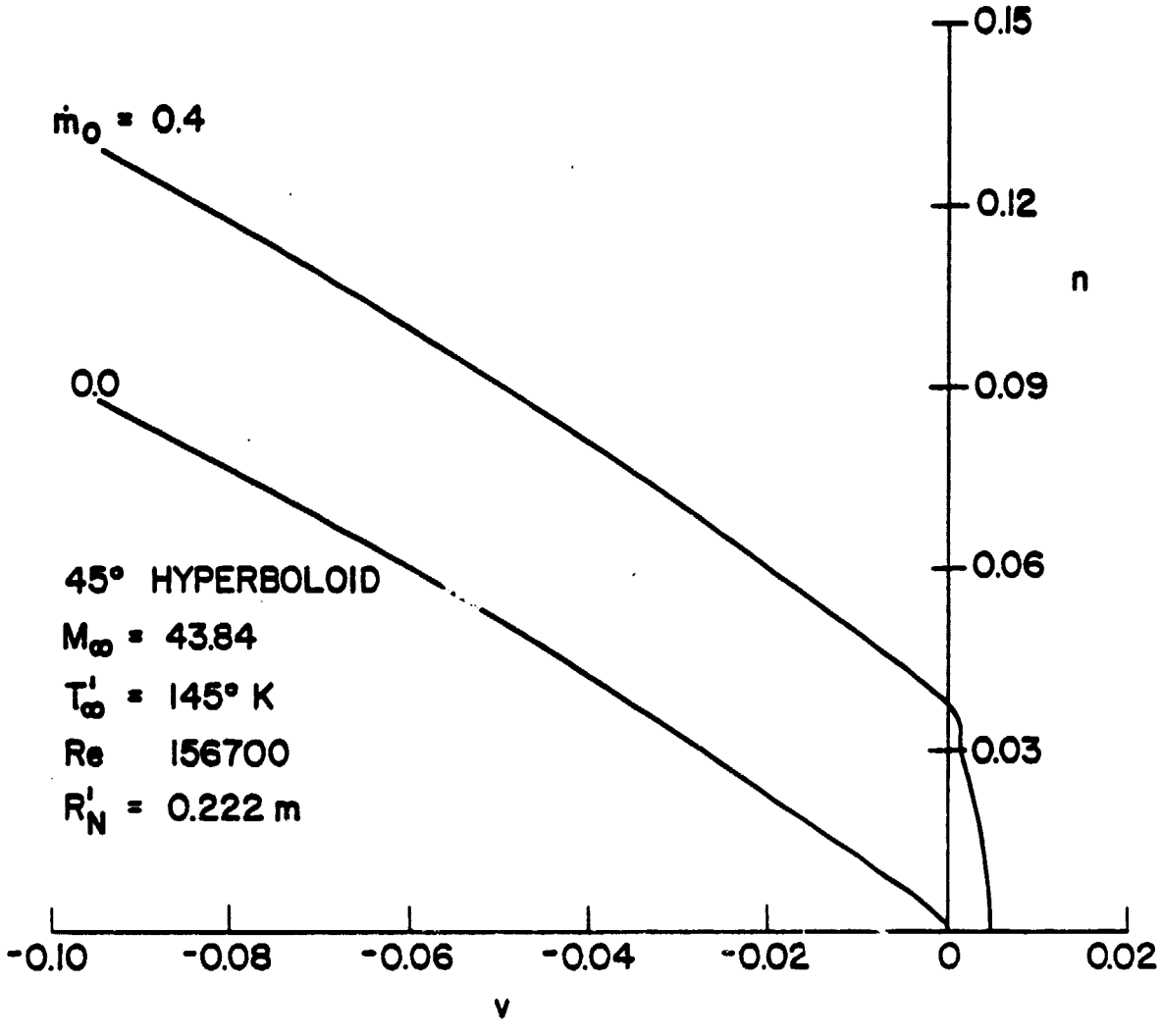

Figure 15. Normal velocity profile variation with surface blowing at s = 0.19635.

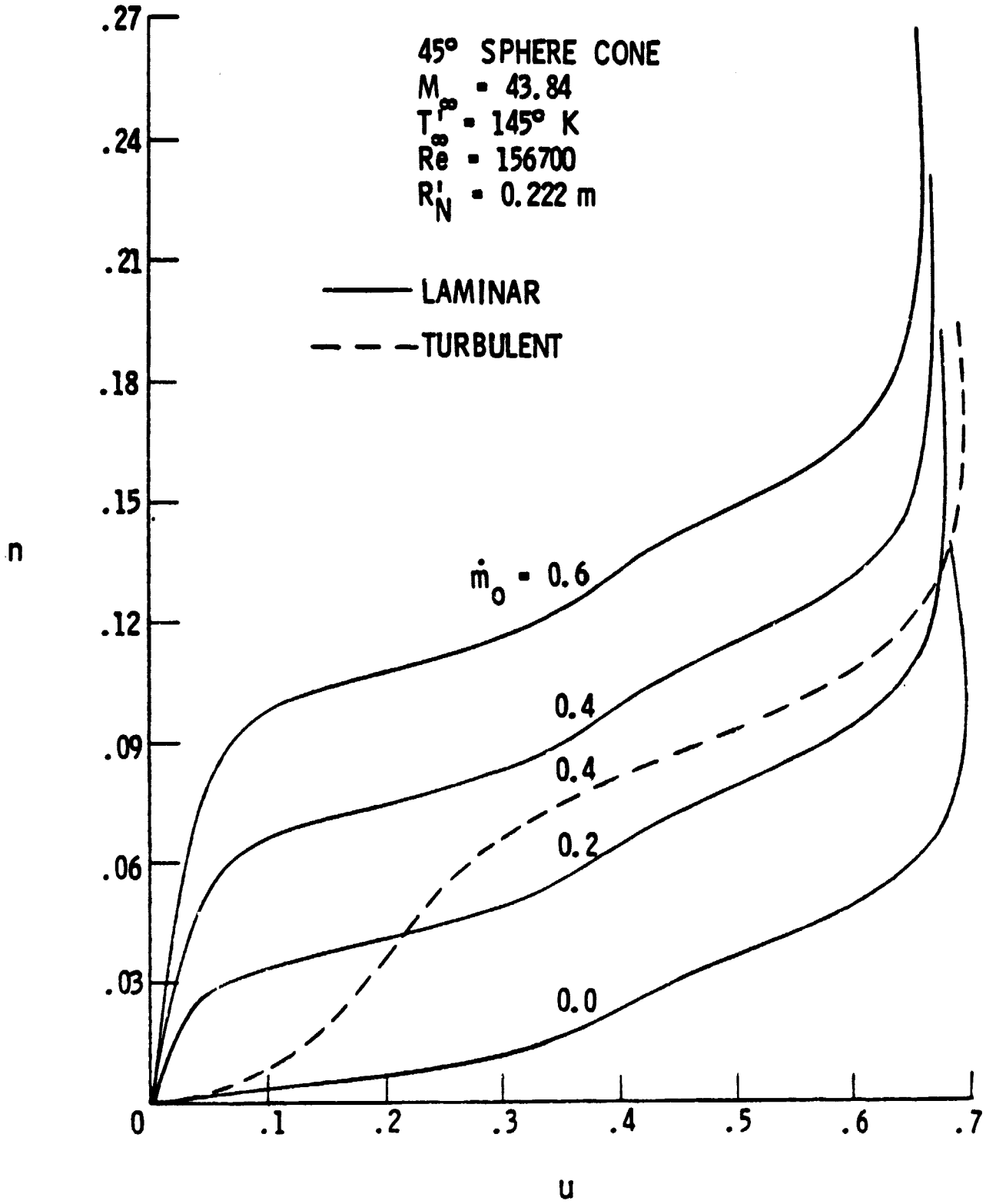

Figure 16. Tangential velocity profile variation with surface blowing at s = 1.76715.

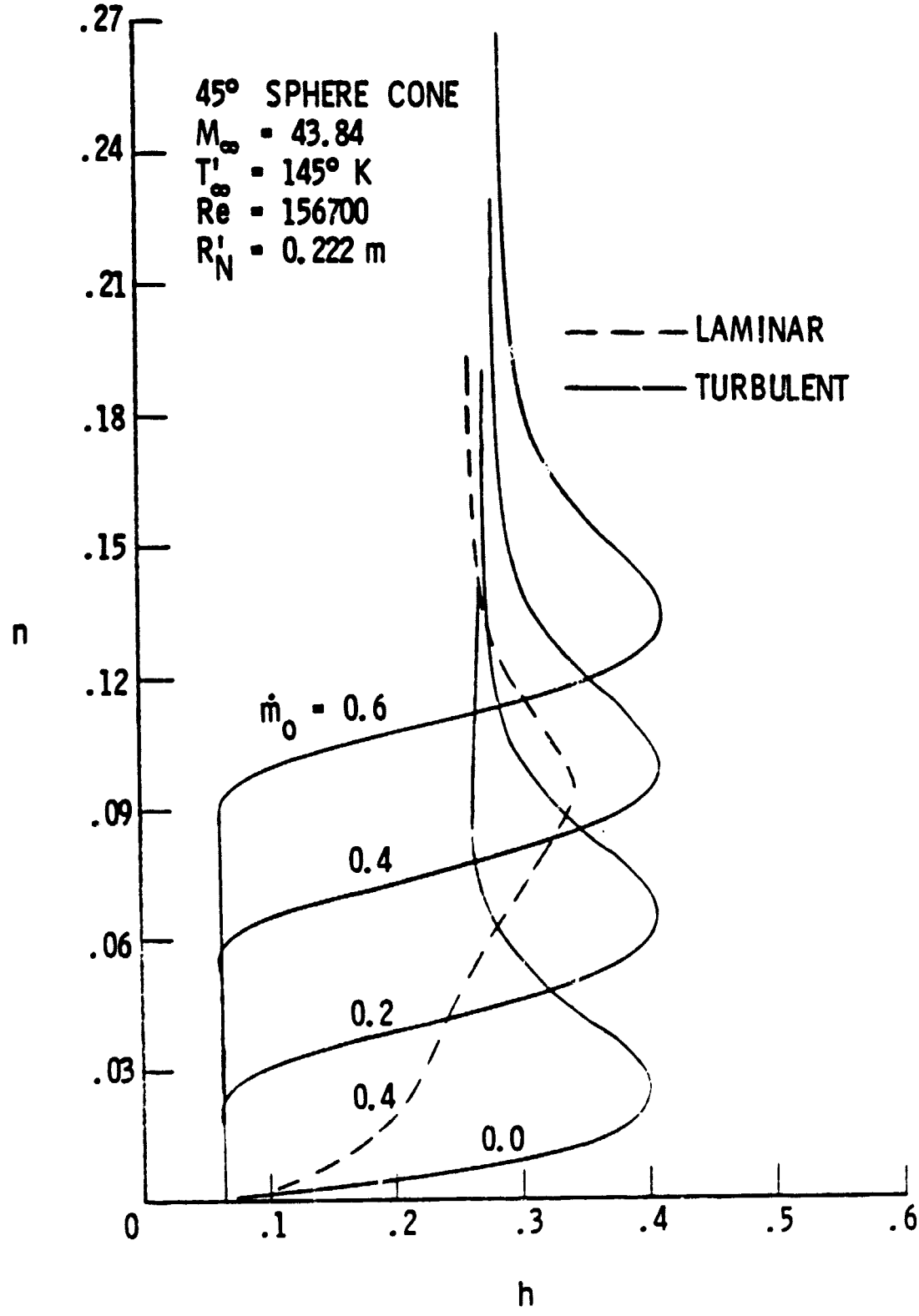

Figure 17. Enthalpy profile variation with surface blowing at s = 1.76715.

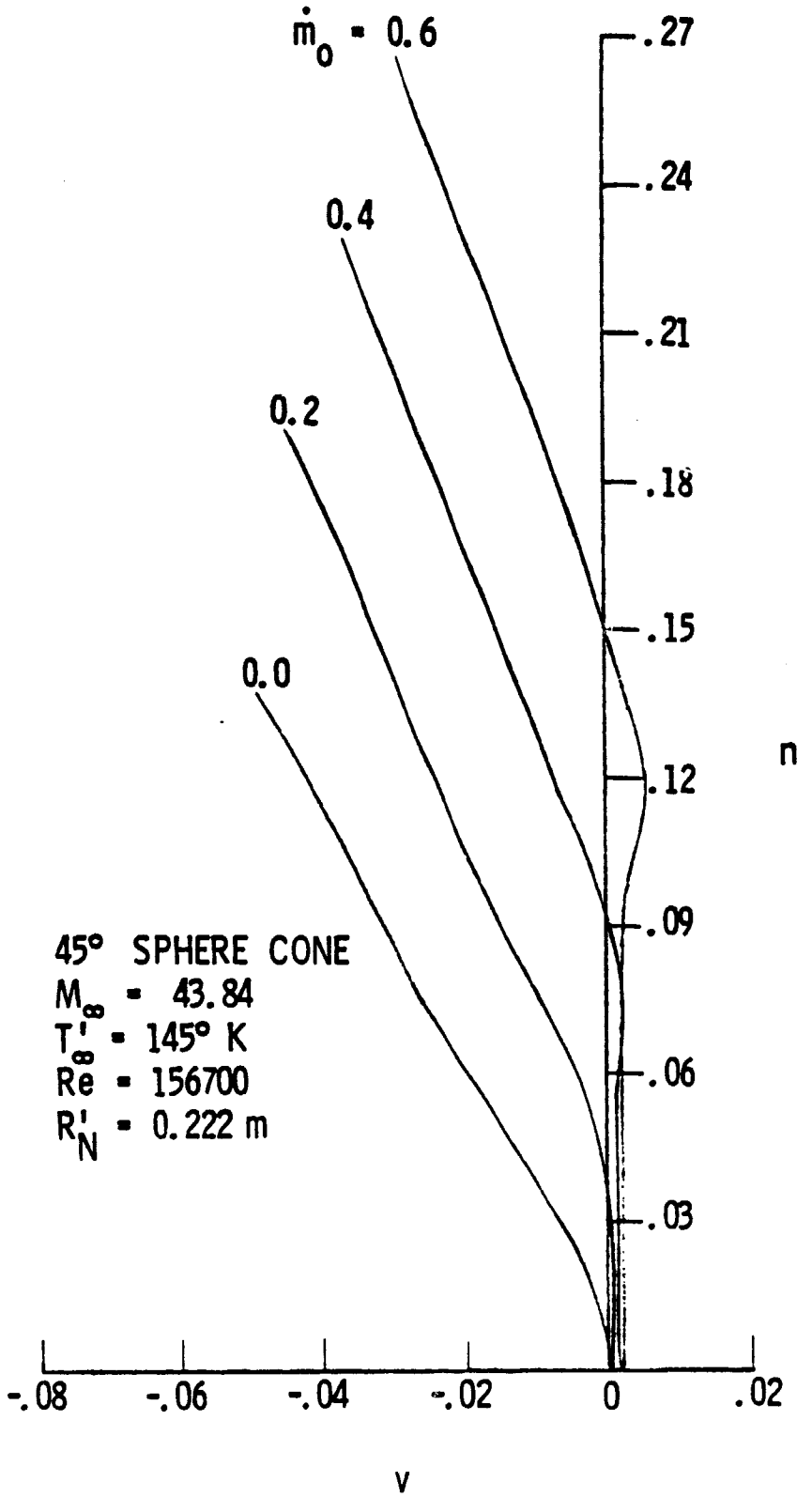

Figure 18. Normal velocity profile variation with surface blowing at s = 1.76715.

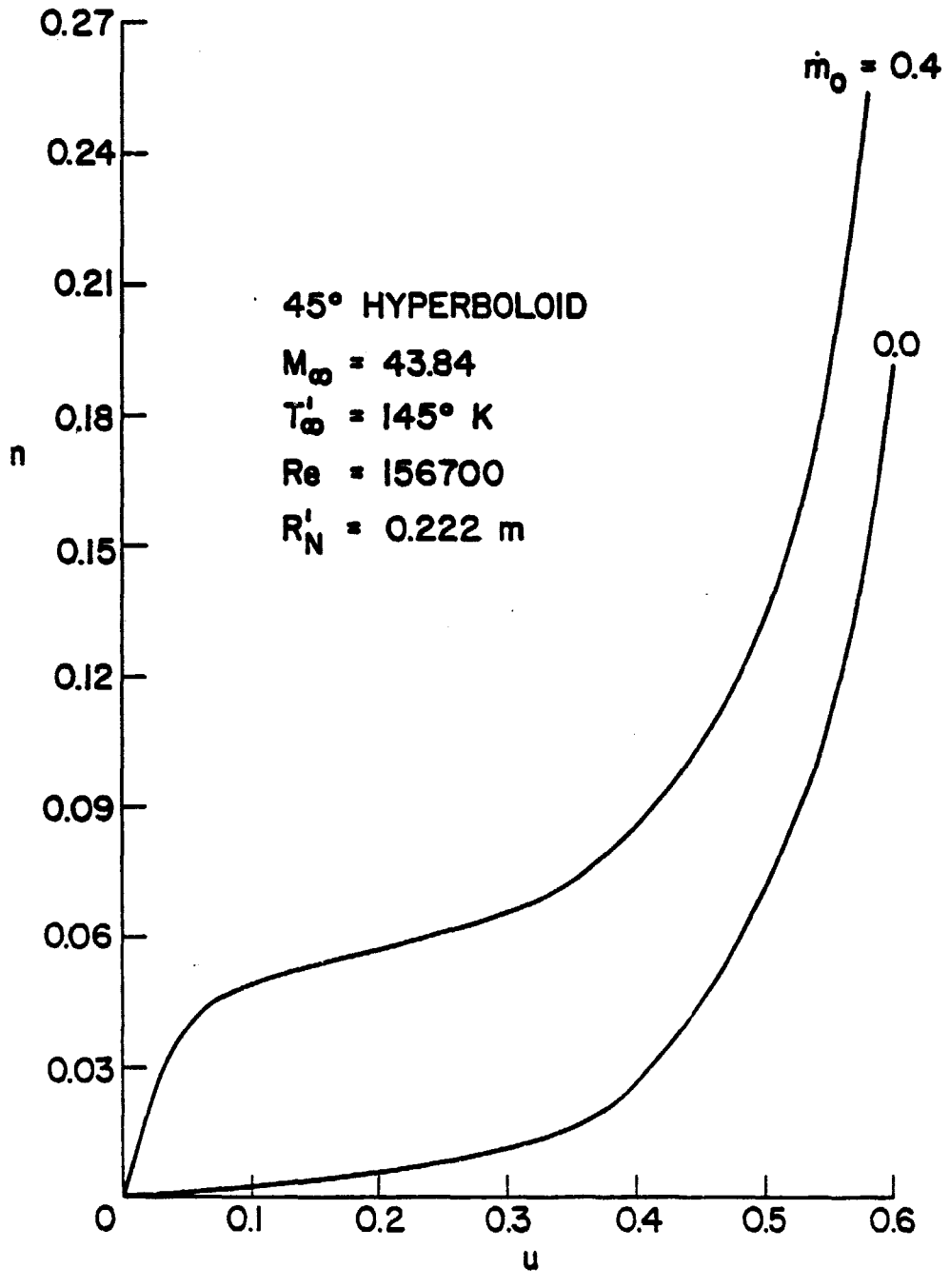

Figure 19. Tangential velocity profile variation with surface blowing at s = 1.76715.

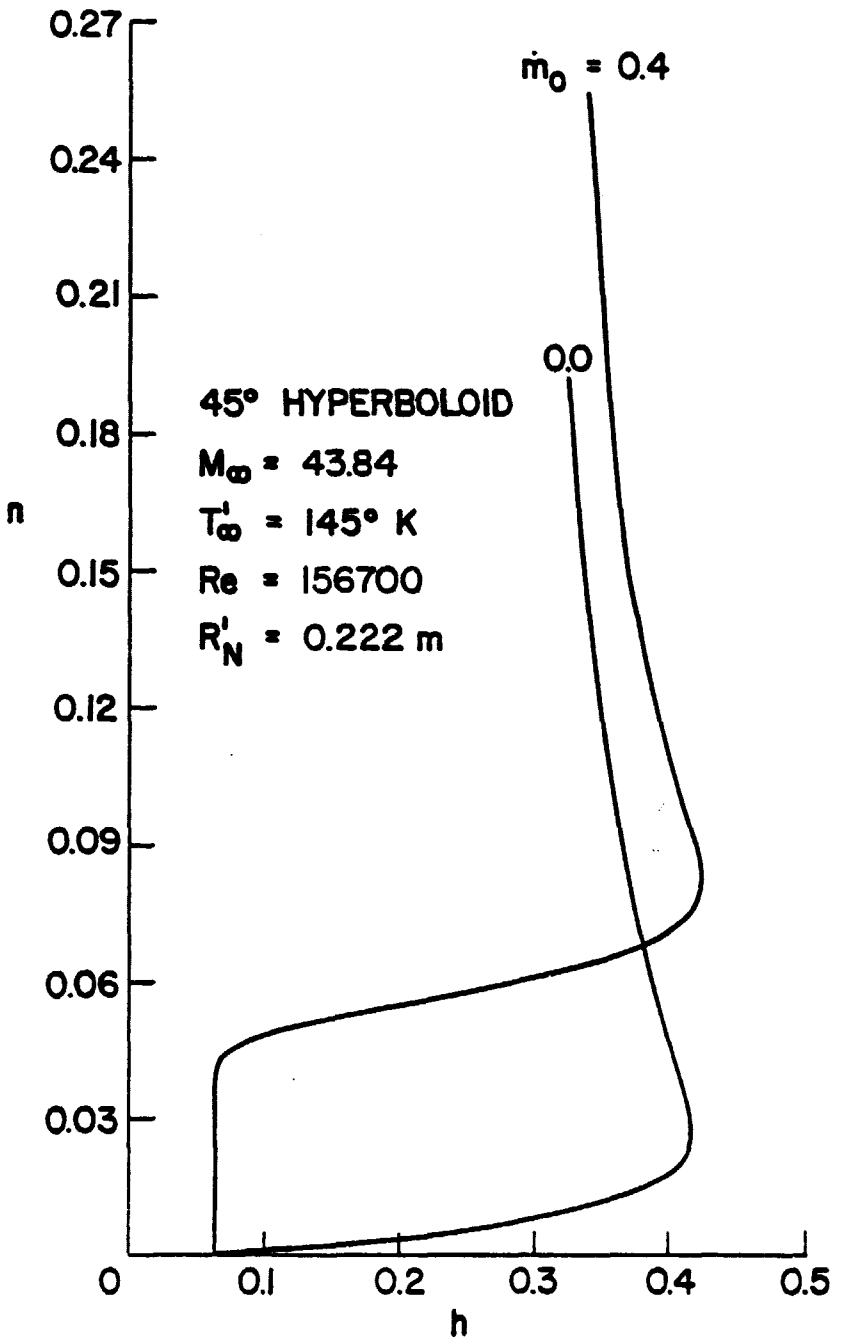

Figure 20. Enthalpy profile variation with surface blowing at s = 1.76715.

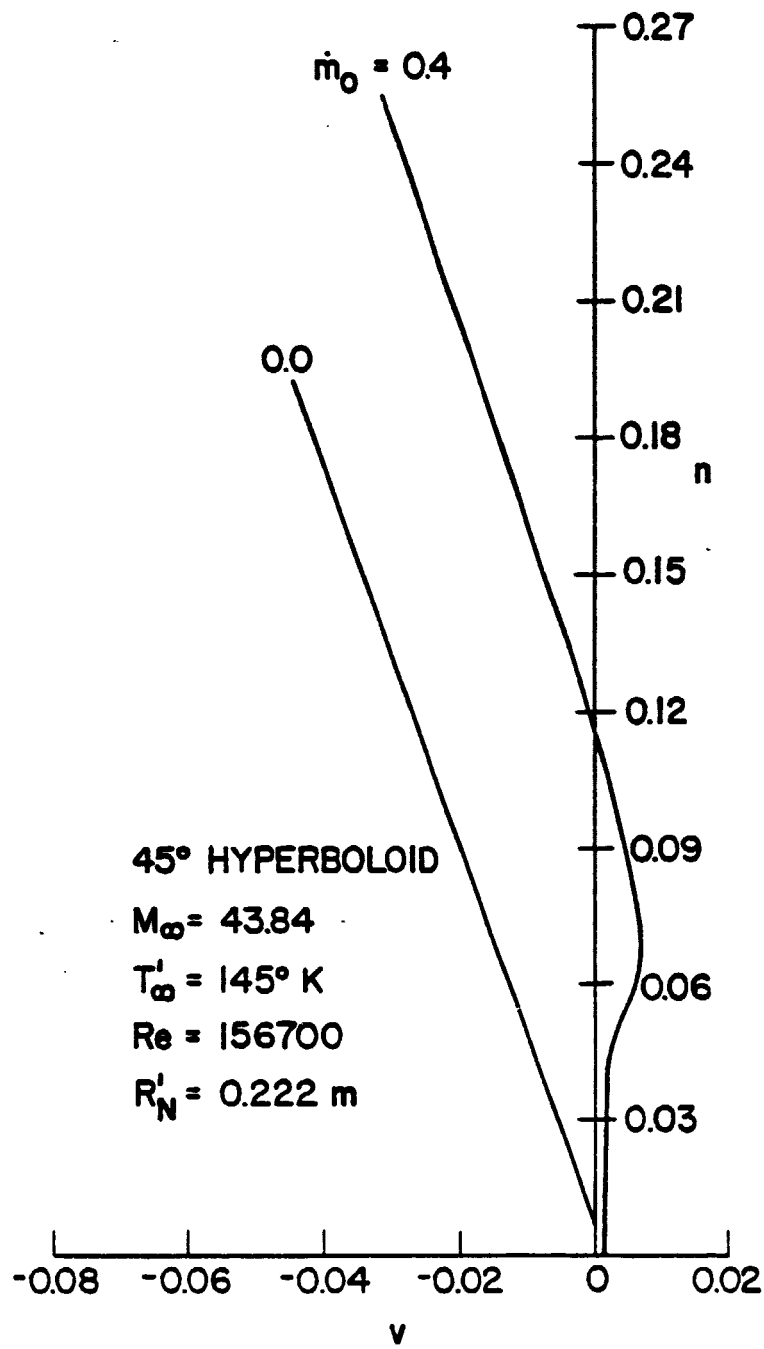

Figure 21. Normal velocity profile variation with surface blowing at s = 1.76715.

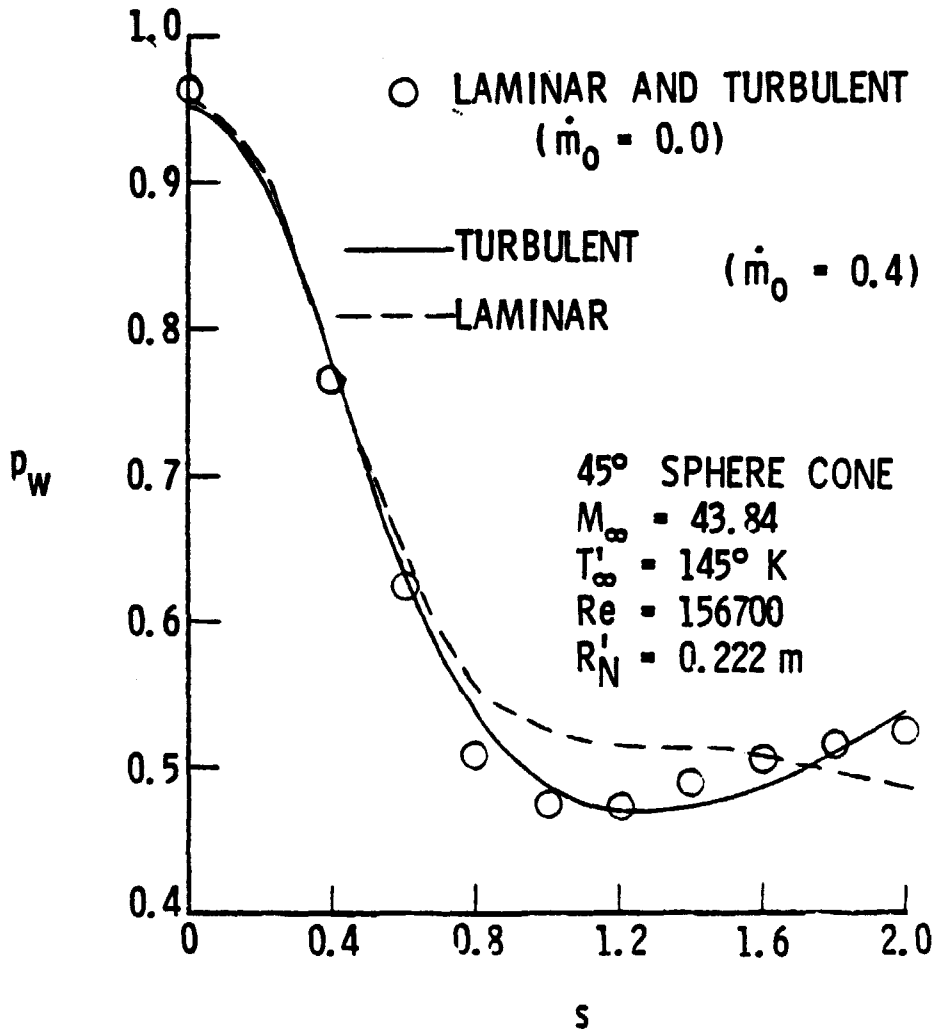

Figure 22. Surface pressure distribution for laminar and turbulent flows with surface blowing.

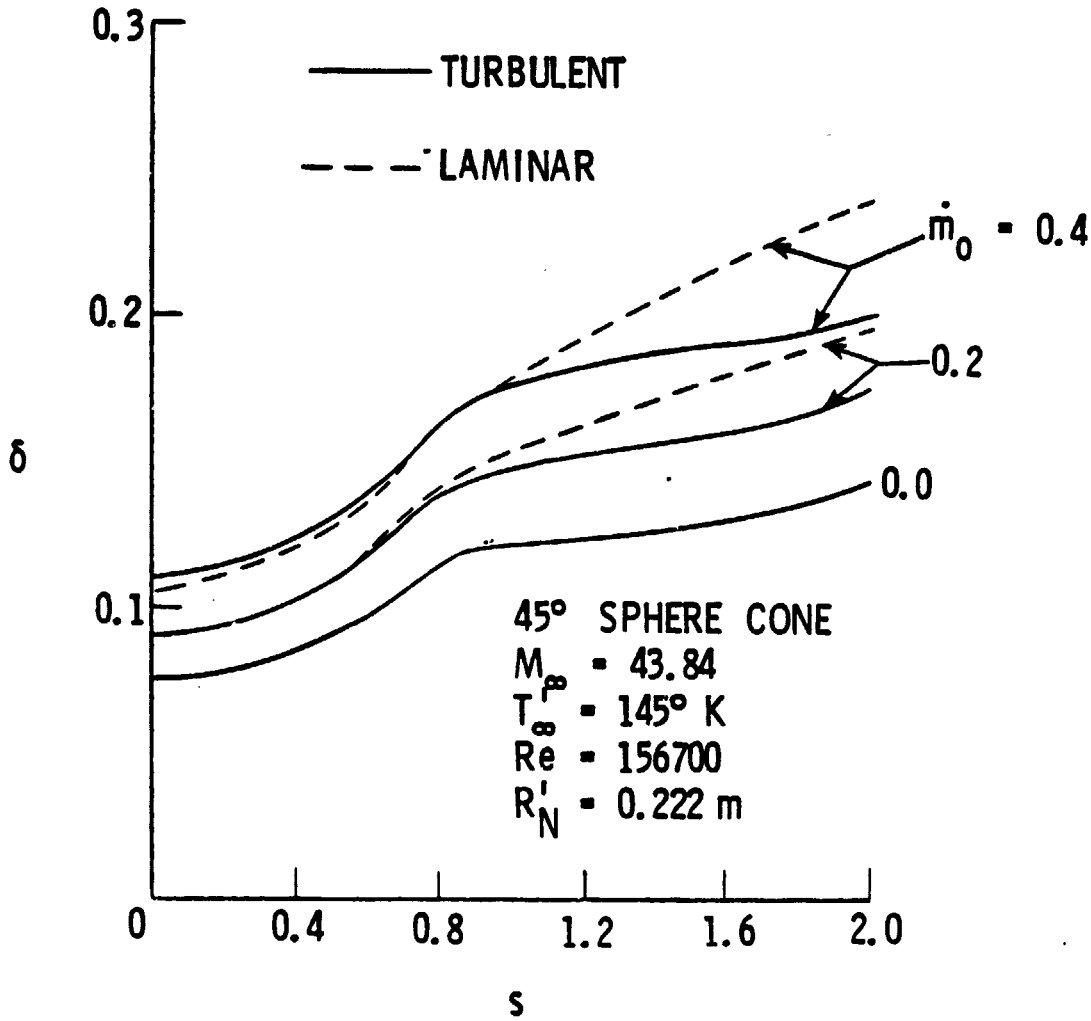

Figure 23. Shock standoff distances for laminar and turbulent flows with surface blowing.

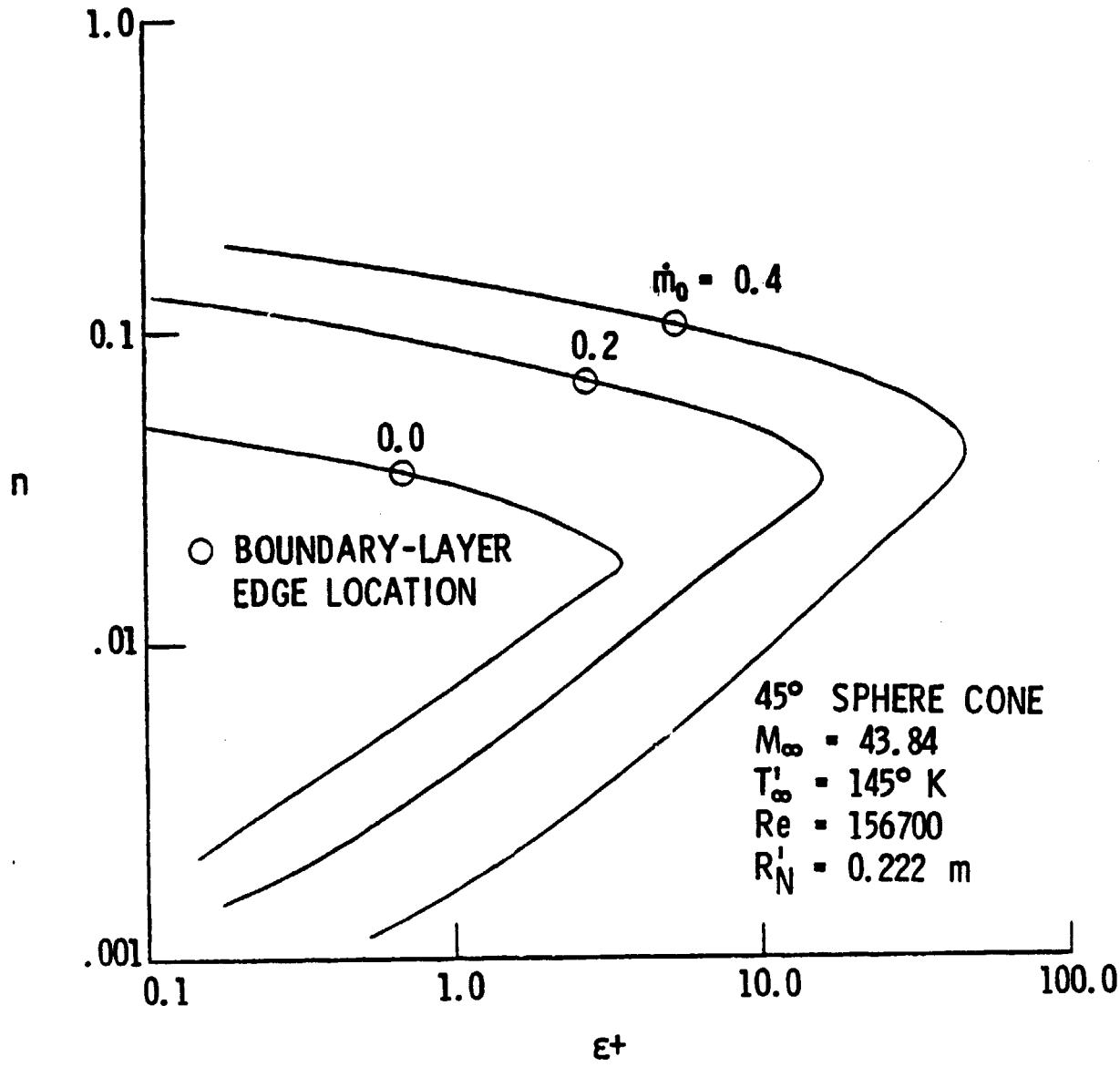

Figure 24. Eddy viscosity profile variation with surface blowing at s = 1.76715.